공학석사 학위논문

Unified Code Calibration for Short- to Medium-span and Long-span Bridges with New Vehicular Live Load Model

새로운 차량활하중 모형을 적용한 일반교량과 장경간교량에 대한 통합 코드캘리브레이션

2018년 2월

서울대학교 대학원

건설환경공학부

김 세 상

ABSTRACT

Unified Code Calibration for Short- to Medium-span and Long-span Bridges with New Vehicular Live Load Model

Sesang Kim
Civil and Environmental Engineering
The Graduate School
Seoul National University

There are two bridge design codes in Korea adopting reliability-based load-and-resistance factor design for short- to medium-span and long-span bridges, respectively. Unified code calibration is required for the bridge design codes since their load-resistance factors were developed separately. Moreover, there is lack of consistency of theoretical backgrounds for a design vehicular live load and the statistical model of a vehicular live load effect. Therefore, the new statistical model of a vehicular live load effect and the corresponding design lane load are proposed based on the same data and the unified code calibration is conducted for the Ultimate Limit State I and V applying the current and new statistical models of the vehicular live load effect. The calibration is performed by adopting the

optimization scheme for uniformly satisfying a target level of reliability. Load factors of the Ultimate Limit State I are defined depending on load compositions so the suggested load-resistance factors are applicable to design not only short- to medium-span but also long-span bridges. Furthermore, calibrations of the Ultimate Limit State V are conducted for short- to medium-span and long-span bridges, respectively. Reliability indices evaluated by proposed load-resistance factors more uniformly satisfy the target reliability index than those calculated by load-resistance factors in the current bridge design codes.

Keywords : code calibration, load-resistance factors, Ultimate Limit state I, Ultimate Limit State V, Korean Highway Bridge Design Code (Limit State Design), statistical model of vehicular live load effect, short- to medium-span bridges, long-span bridges, optimization scheme

Student Number : 2016-21245

TABLE OF CONTENTS

LIST OF FIGURES

LIST OF TABLES

This page intentionally left blank

1. INTRODUCTION

1.1 Motivation

The concept of bridge design codes has changed from allowable stress design (ASD) to reliability-based load-and-resistance factor design (LRFD) and thus load-resistance (L-R) factors should be decided by robust methods. There are two bridge design codes in Korea based on LRFD method: the Korean Highway Bridge Design Code (Limit State Design) (KHBDC) (MOLIT, 2016a) and the Korean Highway Bridge Design Code (Limit State Design) - Cable-supported Bridges (KHBDC-C) (MOLIT, 2016b). The KHBDCs refer to the KHBDC and the KHBDC-C together in this study. The KHBDC-C was written for designing long-span bridges while the KHBDC was produced for short- to medium-span bridges. Unified code calibration is required for the KHBDCs since the L-R factors of the KHBDC and the KHBDC-C were developed separately.

In the studies of Ellingwood *et al*. (1980) and Nowak (1999), the calibrations of L-R factors for building structures and bridges, respectively, were performed adopting reliability-based methods. However, the proposed L-R factors could not apply to design all sizes or types of bridges since they carried out the calibrations based on specific scales. Lee *et al*. (2017) was conducted the calibration of gravitational loads-governed limit states for the AASHTO LRFD Bridge Design Specifications (AASHTO specifications) (AASHTO, 2014) by proposing an

optimization scheme. They normalized a linear limit state to the total nominal load effect so the proposed L-R factors were applicable to design any size or type of bridges. Furthermore, the uniform reliability index to a target reliability was assured across load compositions. However, they only considered the load compositions of short- to medium-span bridges and thus it is required to include the load compositions for long-span bridges in the calibration. Therefore, the unified calibration is performed by taking into account long-span as well as short- to medium-span bridges in this study.

Hwang (2012) proposed the design vehicular live load model for the KHBDC-C while Lee (2014) suggested the statistical model of the vehicular live load effect for the KHBDC-C. Therefore, there is lack of consistency of theoretical backgrounds for the design vehicular live load model and the statistical model of the vehicular live load effect. Calibration should be performed with the statistical model of the vehicular live load effect proposed by considering the corresponding design vehicular live load model since the design vehicular live load model is multiplied by the live load factor. Moreover, the live load factor is decided by applying the statistical model of the vehicular live load effect. On the other hand, Kim (2015) proposed statistical characteristics of the vehicular live load effect taking into account the corresponding vehicular live load model but the assumption to decide the distribution type of the vehicular live load effect was unverified.

1.2 Objectives and Scope

The unified code calibration is performed by applying the optimization scheme developed by Lee *et al*. (2017) for uniformly satisfying a target level of reliability. Calibrations are conducted for the Ultimate Limit State I (ULS-I) and V (ULS-V). The ULS-I and Ultimate Limit State IV (ULS-IV) are gravitational loads-governed limit states in the KHBDCs and, here, the ULS-I is selected as a representative limit state governed by gravitational loads in this study. The proposed L-R factors are applicable to design not only short- to medium-span but also long-span bridges since they are defined depending on load compositions. The resistance factors for reinforced concrete (RC), steel (ST), and prestressed concrete (PC) members are suggested for moment and shear and they are constant in all load compositions.

For calibrations, the statistical model of the vehicular live load effect is proposed and the corresponding design lane load is also suggested based on the same data. The current and proposed statistical models of the vehicular live load effect are applied for calibrations, respectively. The target reliability indices for the ULS-I and V are both set to 3.72 and only load effects induced by major load components in each limit state are considered for each calibration because the load effects caused by the other loads are generally ignored in a calibration. The major load components for the ULS-I are dead and vehicular live loads and those for the ULS-V are dead, vehicular live, and wind loads.

1.3 Organization

In this chapter, the study is briefly introduced. Chapter 2 describes the optimization scheme developed by Lee *et al*. (2017) with introducing normalization of limit state functions and the optimization methods are defined for calibrations of the ULS-I and V. Chapter 3 presents the new statistical models of the vehicular live load and its effect and the corresponding design lane load and multiple presence factor are proposed. In Chapter 4, the calibration of the ULS-I is conducted applying the current and new statistical models of the vehicular live load effect and suggested L-R factors are given with results of reliability analyses. Chapter 5 describes the calibration of the ULS-V using statistical models of the wind load effect induced by the wind velocity of 25m/s and applying the current and new statistical models of the vehicular live load effect. Proposed L-R factors also come out with results of reliability analyses. Lastly, conclusion of this study is presented in Chapter 6.

2. OPTIMIZATION SCHEME FOR CALIBRATION

In this study, calibrations are conducted adopting the optimization scheme developed by Lee *et al*. (2017) for uniformly securing a target reliability index. The optimization scheme is introduced for the ULS-I and its application is extended to the ULS-V in this chapter. For calibrating L-R factors applicable to any type or size of bridges, a limit state function is normalized by the total nominal load effect and the optimization problem is defined based on the normalization.

2.1 Normalization of Limit State Functions

A design equation for LRFD is given as follows (AASHTO, 2014; MOLIT, 2016a; MOLIT, 2016b):

$$\phi S_0 = \sum_i \gamma_i (Q_i)_0 \tag{2.1}$$

where S and Q_i are the resistance of a structural member and the load effect induced by the *i*-th load component, respectively, and ϕ and γ_i are the corresponding resistance and load factors, respectively. A variable with the subscript 0 indicates the nominal value of the variable. The limit state function G for the design equation of Eq. (2.1) is

$$G = S - \sum_i Q_i = 0 \tag{2.2}$$

where the resistance and all load effects are random variables (Haldar and Mahadevan, 2000). The reliability index of the limit state function is calculated by the advanced first-order second-moment method (AFOSM) (Haldar and Mahadevan, 2000). Furthermore, statistical parameters of the equivalent normal distribution of a non-normal random variable are approximately computed by adopting the Rackwitz-Fiessler method (Rackwitz and Fiessler, 1978).

It is required to normalize a limit state function by the total nominal load effect for conducting the unified code calibration since the limit state function becomes dimensionless. The total nominal load effect is as follows:

$$C_0 = \sum_i Q_i \tag{2.3}$$

The normalized limit state function $\overline{G}$ is

$$\overline{G} = \frac{S}{C_0} - \sum_i \frac{Q_i}{C_0} = 0 \rightarrow \overline{G} = \overline{S} - \sum_i \overline{Q_i} = 0 \tag{2.4}$$

where the variables over which bars place denote the normalized variables. A bias factor, a coefficient of variation (COV) and a distribution type of a normalized random variable are equal to those of the orignial random variable. In addition, the reliability indices of Eqs. (2.2) and (2.4) are identical by the theory of the AFOSM (Haldar and Mahadevan, 2000).

2.1.1 Normalization of Ultimate Limit State I

The ULS-I mainly consists of dead and vehicular live load effects so two variables are defined to represent load compositions of the limit state. The dead load ratio which is the ratio of the total nominal dead load effect to the total nominal load effect is given as (Lee *et al*., 2017):

$$\xi = \frac{(Q_{DC})_0 + (Q_{DW})_0}{(Q_{DC})_0 + (Q_{DW})_0 + (Q_{LL})_0} \tag{2.5}$$

where *DC*, *DW* denote dead loads of structural components and nonstructural attachments and wearing surfaces and utilities, respectively, while *LL* is the vehicular live load including its dynamic impact. In addition, the DC-dead load ratio is the ratio of the load effect induced by the *DC* to the total nominal dead load effect as in the following:

$$\eta = \frac{(Q_{DC})_0}{(Q_{DC})_0 + (Q_{DW})_0} \tag{2.6}$$

The normalized nominal load effects and resistance are expressed as follows:

$$(\overline{Q_{DC}})_0 = \xi\eta \tag{2.7a}$$

$$(\overline{Q_{DW}})_0 = \xi(1-\eta) \tag{2.7b}$$

$$(\overline{Q_{LL}})_0 = 1-\xi \tag{2.7c}$$

$$\overline{S}_0 = \frac{1}{\phi}\sum_i \gamma_i (\overline{Q_i})_0 = \frac{1}{\phi}\left(\gamma_{DC}\xi\eta + \gamma_{DW}\xi(1-\eta) + \gamma_{LL}(1-\xi)\right) \tag{2.7d}$$

2.1.2 Normalization of Ultimate Limit State V

Major components of the ULS-V are dead, vehicular live, and wind load effects. The wind load effect is induced by the wind velocity of 25m/s. The dead load effect, which is sum of load effects caused by *DC* and *DW*, is assumed to be zero for applying the optimization scheme proposed by Lee *et al*. (2017) with four load effects and this assumption is verified by load compositions of existing bridges in Section 5.2.

Two variables are defined to represent load compositions of the limit state. The wind load ratio which is the ratio of the nominal wind load effect induced by the wind velocity of 25m/s to the total nominal load effect is given as:

$$\chi = \frac{(Q_{WS_{25}})_0}{(Q_{DC})_0 + (Q_{DW})_0 + (Q_{LL})_0 + (Q_{WS_{25}})_0} \tag{2.8}$$

where WS_{25} denotes the wind load caused by the wind velocity of 25m/s. In addition, the DC-total load ratio is the ratio of the load effect induced by the *DC* to the total nominal load effect as in the following:

$$\theta = \frac{(Q_{DC})_0}{(Q_{DC})_0 + (Q_{DW})_0 + (Q_{LL})_0 + (Q_{WS_{25}})_0} \tag{2.9}$$

The normalized nominal load effects and resistance are expressed as follows:

$$(\overline{Q_{DC}})_0 = \theta \tag{2.10a}$$

$$(\overline{Q_{DW}})_0 = -\theta \tag{2.10b}$$

$$(\overline{Q_{LL}})_0 = 1-\chi \tag{2.10c}$$

$$(\overline{Q_{WS_{25}}})_0 = \chi \tag{2.10d}$$

$$\overline{S}_0 = \frac{1}{\phi}\sum_i \gamma_i (\overline{Q_i})_0 = \frac{1}{\phi}\left(\gamma_{DC}\theta + \gamma_{DW}(-\theta) + \gamma_{LL}(1-\chi) + \gamma_{WS_{25}}\chi\right) \tag{2.10e}$$

2.2 Optimization for Calibration

For calibration of L-R factors, an object function is defined. Solving the object function, L-R factors are calculated by minimizing differences between a target reliability index and the reliability index evaluated by the L-R factors over entire ranges of load compositions.

2.2.1 Object Function for Ultimate Limit State I

The object function for the ULS-I is defined as (Lee *et al.*, 2017)

$$\underset{\boldsymbol{\phi},\boldsymbol{\gamma}}{\text{Min}}\Pi = \frac{1}{2}\int_{L_\xi}^{U_\xi}\int_{L_\eta}^{U_\eta} (\boldsymbol{\beta}(\xi,\eta,\boldsymbol{\phi},\boldsymbol{\gamma}) - \beta_T \mathbf{1})^T (\boldsymbol{\beta}(\xi,\eta,\boldsymbol{\phi},\boldsymbol{\gamma}) - \beta_T \mathbf{1}) d\eta d\xi \tag{2.11}$$

where $\boldsymbol{\phi} = (\phi^{\mathrm{RC}}, \phi^{\mathrm{ST}}, \phi^{\mathrm{PC}})^T$, in which ϕ^p is the resistance factor of a member type p, while $\boldsymbol{\gamma} = (\gamma_{DC}, \gamma_{DW}, \gamma_{LL})^T$, in which γ_i is the load factor of the *i*-th load component, and $\mathbf{1}$ denotes a column vector whose components are all unit values. $\beta(\xi,\eta,\phi^p,\boldsymbol{\gamma})$ is the reliability index evaluated by AFOSM depending on variables

in the parentheses and β_T is a target reliability index. U_x and L_x are the upper and the lower bounds of a variable x, respectively. Optimized L-R factors are calculated by solving Eq. (2.11).

2.2.2 Object Function for Ultimate Limit State V

The object function for the ULS-V is defined as follows:

$$\underset{\boldsymbol{\gamma}}{\text{Min}}\Pi = \frac{1}{2}\int_{L_\chi}^{U_\chi}\int_{L_\theta}^{U_\theta}(\boldsymbol{\beta}(\chi,\theta,\boldsymbol{\phi},\boldsymbol{\gamma}) - \beta_T\mathbf{1})^T(\boldsymbol{\beta}(\chi,\theta,\boldsymbol{\phi},\boldsymbol{\gamma}) - \beta_T\mathbf{1})d\theta d\chi \qquad (2.12)$$

where $\boldsymbol{\phi} = (\phi^{\text{RC}}, \phi^{\text{ST}}, \phi^{\text{PC}})^T$, whose values are proposed in the calibration of the ULS-I, while $\boldsymbol{\gamma} = (\gamma_{DC}, \gamma_{DW}, \gamma_{LL}, \gamma_{WS_{25}})^T$, in which load factors of *DC* and *DW* are suggested in the calibration of the ULS-I. $\beta(\chi,\theta,\phi^p,\boldsymbol{\gamma})$ is the reliability index evaluated by AFOSM depending on variables in the parentheses. Optimized load factors of *LL* and WS_{25} are calculated by solving Eq. (2.12).

2.2.3 Calculation of Optimization Problem

The optimization problem is solved by the first-order necessary condition of the object function of Eq. (2.11) or (2.12). Variation of the object function with respect to $\mathbf{x} = (\boldsymbol{\phi}^T, \boldsymbol{\gamma}^T)^T$ is taken as Eq. (2.13a) or (2.13b) (Lee *et al*., 2017).

$$\delta_{\mathbf{x}}\Pi = \int_{L_\xi}^{U_\xi}\int_{L_\eta}^{U_\eta}\delta_{\mathbf{x}}\boldsymbol{\beta}^T(\boldsymbol{\beta} - \beta_T\mathbf{1})d\eta d\xi = 0 \qquad (2.13a)$$

$$\delta_{\mathbf{x}}\Pi = \int_{L_\chi}^{U_\chi}\int_{L_\theta}^{U_\theta} \delta_{\mathbf{x}}\boldsymbol{\beta}^T(\boldsymbol{\beta} - \beta_T\mathbf{1})d\theta d\chi = 0 \tag{2.13b}$$

where $\delta_{\mathbf{x}}$ denotes the operator of variation with respect to $\mathbf{x}$. It is needed to solve Eq. (2.13a) or (2.13b) repetitively because the reliability index is a nonlinear function of the vector of L-R factors, $\mathbf{x}$. For solving the nonlinear equation, the reliability index vector is approximately computed by the first-order Taylor expansion (Lee *et al*., 2017).

$$\begin{aligned} \delta_{\mathbf{x}}\boldsymbol{\beta} &= \frac{\partial\boldsymbol{\beta}}{\partial\boldsymbol{\phi}}\delta\boldsymbol{\phi} + \frac{\partial\boldsymbol{\beta}}{\partial\boldsymbol{\gamma}}\delta\boldsymbol{\gamma} = \overline{\mathbf{h}}^{\phi}\delta\boldsymbol{\phi} + \overline{\mathbf{h}}^{\gamma}\delta\boldsymbol{\gamma} \\ \boldsymbol{\beta}_{j+1} &\approx \boldsymbol{\beta}_j(\mathbf{x}_j) + \frac{\partial\boldsymbol{\beta}}{\partial\boldsymbol{\phi}}\Delta\boldsymbol{\phi} + \frac{\partial\boldsymbol{\beta}}{\partial\boldsymbol{\gamma}}\Delta\boldsymbol{\gamma} = \boldsymbol{\beta}_j + \overline{\mathbf{h}}^{\phi}\Delta\boldsymbol{\phi} + \overline{\mathbf{h}}^{\gamma}\Delta\boldsymbol{\gamma} \end{aligned} \tag{2.14}$$

where the subscript j denotes the iteration count, and $\boldsymbol{\beta}_j(\mathbf{x}_j)$ is the reliability index vector evaluated by the L-R factors calculated from the *j*-th iteration. The sensitivities of reliability index vector with respect to the L-R factors are computed by the direct differentiation method. It is as Eq. (2.15a) or (2.15b) to substitute Eq. (2.14) into Eq. (2.13a) or (2.13b) (Lee *et al*., 2017):

$$
\begin{aligned}
\delta_{\mathbf{x}}\Pi &= \int_{L_\xi}^{U_\xi}\int_{L_\eta}^{U_\eta}\left(\bar{\mathbf{h}}^{\phi}\delta\boldsymbol{\phi}+\bar{\mathbf{h}}^{\gamma}\delta\boldsymbol{\gamma}\right)^T\left(\boldsymbol{\beta}_j+\bar{\mathbf{h}}^{\phi}\Delta\boldsymbol{\phi}+\bar{\mathbf{h}}^{\gamma}\Delta\boldsymbol{\gamma}-\beta_T\mathbf{1}\right)d\eta d\xi \\
&= \int_{L_\xi}^{U_\xi}\int_{L_\eta}^{U_\eta}\left(\delta\boldsymbol{\phi}^T,\delta\boldsymbol{\gamma}^T\right)\mathbf{h}\begin{pmatrix}\Delta\boldsymbol{\phi}\\ \Delta\boldsymbol{\gamma}\end{pmatrix}d\eta d\xi+\int_{L_\xi}^{U_\xi}\int_{L_\eta}^{U_\eta}\left(\delta\boldsymbol{\phi}^T,\delta\boldsymbol{\gamma}^T\right)\mathbf{b}d\eta d\xi \\
&= \int_{L_\xi}^{U_\xi}\int_{L_\eta}^{U_\eta}\delta\mathbf{x}^T\mathbf{h}\Delta\mathbf{x}d\eta d\xi+\int_{L_\xi}^{U_\xi}\int_{L_\eta}^{U_\eta}\delta\mathbf{x}^T\mathbf{b}d\eta d\xi \\
&= \delta\mathbf{x}^T\left(\int_{L_\xi}^{U_\xi}\int_{L_\eta}^{U_\eta}\mathbf{h}d\eta d\xi\Delta\mathbf{x}+\int_{L_\xi}^{U_\xi}\int_{L_\eta}^{U_\eta}\mathbf{b}d\eta d\xi\right) \\
&= \delta\mathbf{x}^T\left(\mathbf{H}_{\xi\eta}\Delta\mathbf{x}+\mathbf{B}_{\xi\eta}\right)=0
\end{aligned}
\tag{2.15a}
$$

$$
\begin{aligned}
\delta_{\mathbf{x}}\Pi &= \int_{L_\chi}^{U_\chi}\int_{L_\theta}^{U_\theta}\left(\bar{\mathbf{h}}^{\phi}\delta\boldsymbol{\phi}+\bar{\mathbf{h}}^{\gamma}\delta\boldsymbol{\gamma}\right)^T\left(\boldsymbol{\beta}_j+\bar{\mathbf{h}}^{\phi}\Delta\boldsymbol{\phi}+\bar{\mathbf{h}}^{\gamma}\Delta\boldsymbol{\gamma}-\beta_T\mathbf{1}\right)d\theta d\chi \\
&= \int_{L_\chi}^{U_\chi}\int_{L_\theta}^{U_\theta}\left(\delta\boldsymbol{\phi}^T,\delta\boldsymbol{\gamma}^T\right)\mathbf{h}\begin{pmatrix}\Delta\boldsymbol{\phi}\\ \Delta\boldsymbol{\gamma}\end{pmatrix}d\theta d\chi+\int_{L_\chi}^{U_\chi}\int_{L_\theta}^{U_\theta}\left(\delta\boldsymbol{\phi}^T,\delta\boldsymbol{\gamma}^T\right)\mathbf{b}d\theta d\chi \\
&= \int_{L_\chi}^{U_\chi}\int_{L_\theta}^{U_\theta}\delta\mathbf{x}^T\mathbf{h}\Delta\mathbf{x}d\theta d\chi+\int_{L_\chi}^{U_\chi}\int_{L_\theta}^{U_\theta}\delta\mathbf{x}^T\mathbf{b}d\theta d\chi \\
&= \delta\mathbf{x}^T\left(\int_{L_\chi}^{U_\chi}\int_{L_\theta}^{U_\theta}\mathbf{h}d\theta d\chi\Delta\mathbf{x}+\int_{L_\chi}^{U_\chi}\int_{L_\theta}^{U_\theta}\mathbf{b}d\theta d\chi\right) \\
&= \delta\mathbf{x}^T\left(\mathbf{H}_{\chi\theta}\Delta\mathbf{x}+\mathbf{B}_{\chi\theta}\right)=0
\end{aligned}
\tag{2.15b}
$$

where

$$
\mathbf{h}=\begin{bmatrix}(\bar{\mathbf{h}}^{\phi})^T\bar{\mathbf{h}}^{\phi} & (\bar{\mathbf{h}}^{\phi})^T\bar{\mathbf{h}}^{\gamma}\\ (\bar{\mathbf{h}}^{\gamma})^T\bar{\mathbf{h}}^{\phi} & (\bar{\mathbf{h}}^{\gamma})^T\bar{\mathbf{h}}^{\gamma}\end{bmatrix},\quad \mathbf{b}=\begin{bmatrix}(\bar{\mathbf{h}}^{\phi})^T(\boldsymbol{\beta}_j-\beta_T\mathbf{1})\\ (\bar{\mathbf{h}}^{\gamma})^T(\boldsymbol{\beta}_j-\beta_T\mathbf{1})\end{bmatrix} \tag{2.16}
$$

By solving Eq. (2.15a) or (2.15b), the incremental vector $\Delta\mathbf{x}$ is expressed as:

$$
\mathbf{H}_{\xi\eta}\Delta\mathbf{x}+\mathbf{B}_{\xi\eta}=0\rightarrow\Delta\mathbf{x}=-\mathbf{H}_{\xi\eta}^{-1}\mathbf{B}_{\xi\eta} \tag{2.17a}
$$

$$
\mathbf{H}_{\chi\theta}\Delta\mathbf{x}+\mathbf{B}_{\chi\theta}=0\rightarrow\Delta\mathbf{x}=-\mathbf{H}_{\chi\theta}^{-1}\mathbf{B}_{\chi\theta} \tag{2.17b}
$$

Therefore, the vector of L-R factors $\mathbf{x}$ is updated and converged by iteration with reasonable initial values of $\mathbf{x}$, which are generally set to L-R factors in current codes.

This page intentionally left blank

3. NEW VEHICULAR LIVE LOAD MODEL

A design vehicular live load and the statistical model of the vehicular live load effect should be related to each other since L-R factors are decided applying the statistical model of the vehicular live load effect and the live load factor is multiplied to the design vehicular live load. In this chapter, the design vehicular live load and the statistical model of the vehicular live load effect are dependently proposed based on the same statistical model of the vehicular live load. The suggested statistical model of the vehicular live load effect is used for calibrations in Chapters 4 and 5.

3.1 Statistical Model of Vehicular Live Load

3.1.1 Simulated Data of Vehicular Live Load

Simulated data of a vehicular live load are used for determining the statistical model of the vehicular live load. They are obtained from simulations of the vehicular live load conducted by Kim and Song (2017) based on Weigh-In-Motion (WIM) data measured in Korea. The sites of WIM measurement are Gimcheon, Seonsan, and Waegwan and details of the WIM data are given in Table 3.1. In addition, reference lengths of the simulations are 40, 60, 80, 100, 150, 200, 400, ⋯ , 1800, and 2000m. They provide statistical characteristics of 100-year maximum all

Table 3.1 Details of WIM data (Kim and Song, 2017)

Location	Number of measured lanes	Annual average daily traffic (vehicle/day)	Period of measurement
Gimcheon	3	17,885	Feb. to Dec. 2013
Seonsan	2	29,484	Feb. to Dec. 2013
Waegwan	4	53,595	Feb. to Dec. 2013

axle loads on each lane, which are calculated by extrapolation of 1-year maximum all axle loads on each lane. The 100-year maximum all axle loads on each lane follow generalized extreme value (GEV) distributions and these statistical parameters of Gimcheon, Seonsan, and Waegwan are shown in Table 3.2. k_{gev}, σ_{gev}, and μ_{gev} are the shape, scale, and location parameters of a GEV distribution and L is a reference length in the table. The 100-year maximum all axle loads on a lane are given in kN.

Table 3.2 Statistical parameters of 100-year maximum all axle loads on a lane (Kim and Song, 2017)

L (m)	Gimcheon								
	First lane			Second lane			Third lane		
	k_{gev}	σ_{gev}	μ_{gev}	k_{gev}	σ_{gev}	μ_{gev}	k_{gev}	σ_{gev}	μ_{gev}
40	0.10	103	951	-0.16	17	936	-0.03	40	1039
60	-0.22	24	914	0.39	131	1142	0.36	218	1385
80	-0.17	13	924	0.22	192	1486	-0.05	54	1262
100	0.02	34	985	-0.47	11	1288	-0.06	49	1345
150	0.42	345	1587	0.10	80	1542	0.25	184	1764
200	0.06	109	1404	-0.22	37	1703	0.05	100	1891
400	-0.14	43	1523	-0.10	79	2306	0.10	187	2822
600	0.01	114	1886	-0.05	107	2762	0.10	230	3620
800	-0.07	104	2081	0.07	212	3301	0.12	276	4323
1000	0.07	177	2338	-0.01	165	3567	0.01	228	4911
1200	0.04	189	2560	-0.01	188	3941	-0.15	150	5407
1400	0.01	194	2767	-0.04	181	4239	-0.09	201	6112
1600	0.03	223	2968	-0.03	207	4569	-0.06	254	6775
1800	0.05	249	3153	-0.05	200	4816	-0.03	304	7419
2000	0.01	244	3329	-0.11	173	5052	-0.05	318	8016

Table 3.2 (*Continued*)

L (m)	Seonsan						Waegwan		
	First lane			Second lane			First lane		
	k_{gev}	σ_{gev}	μ_{gev}	k_{gev}	σ_{gev}	μ_{gev}	k_{gev}	σ_{gev}	μ_{gev}
40	0.04	129	1517	-0.02	56	1168	-0.26	33	949
60	-0.24	56	1666	0.00	98	1523	-0.06	34	997
80	-0.12	103	1976	-0.04	90	1709	0.16	133	1308
100	-0.10	137	2287	0.02	131	1983	0.15	157	1476
150	-0.04	221	2979	-0.08	115	2411	0.24	249	1815
200	0.07	388	3702	-0.20	83	2747	0.10	202	2008
400	-0.06	354	5151	-0.07	203	4408	0.17	555	3498
600	0.06	738	7182	0.02	368	5864	0.10	589	4386
800	0.03	851	8732	-0.02	389	7072	0.09	738	5436
1000	-0.01	859	9917	0.02	485	8122	0.03	617	5772
1200	-0.05	827	10805	-0.05	429	8931	0.10	963	7033
1400	-0.08	760	11439	-0.04	485	9846	0.07	926	7540
1600	-0.11	713	12004	0.04	724	11085	0.06	935	7945
1800	-0.08	816	12785	0.02	706	11746	0.06	982	8345
2000	-0.07	874	13379	0.03	761	12543	0.08	1073	8719

Table 3.2 (*Continued*)

L (m)	Waegwan								
	Second lane			Third lane			Fourth lane		
	k_{gev}	σ_{gev}	μ_{gev}	k_{gev}	σ_{gev}	μ_{gev}	k_{gev}	σ_{gev}	μ_{gev}
40	-0.07	95	1381	-0.17	73	1416	-0.17	39	1094
60	-0.06	102	1617	-0.03	127	1815	0.15	155	1492
80	0.13	189	1906	0.20	363	2454	-0.05	90	1596
100	0.18	304	2319	-0.03	181	2403	-0.04	118	1886
150	0.22	502	3111	0.06	341	3265	-0.11	126	2388
200	0.21	628	3792	0.00	336	3775	-0.23	92	2698
400	0.20	1141	6308	-0.01	512	5829	-0.21	149	4226
600	0.16	1340	8046	-0.08	551	7579	-0.21	192	5561
800	0.16	1600	9741	-0.06	728	9326	-0.20	255	6905
1000	0.09	1417	10598	-0.13	614	10349	-0.21	287	8175
1200	0.10	1754	12380	-0.11	793	11985	-0.22	307	8913
1400	0.07	1641	13075	-0.11	861	13081	-0.23	273	8894
1600	0.08	1840	14108	-0.26	636	13961	-0.22	369	10748
1800	0.11	2135	15132	-0.10	950	14644	-0.19	452	11710
2000	0.14	2381	15945	-0.06	1181	15712	-0.15	608	12860

3.1.2 Definition of Vehicular Live Load

The vehicular live load, *LL*, is defined as the average of 100-year maximum uniformly distributed load (UDL) over each lane in this study.

$$LL = \left(\sum_{i=1}^{n} w_i \right) \Big/ n \tag{3.1}$$

where w_i is 100-year maximum UDL of the *i*-th lane and n is the number of loaded lanes. Here, UDL is a sum of all axle loads on a lane divided by a reference length in kN/m. Statistical characteristics of the vehicular live load are decided using statistical parameters in Table 3.2 through Monte Carlo simulation (MCS). It is assumed that all 100-year maximum UDLs of a lane are statistically independent each other.

Waegwan is determined as the representative region for the vehicular live load since the mean of the vehicular live load of Waegwan is similar to that of Seonsan and greater than that of Gimcheon. Furthermore, the decreasing rate of the mean of the vehicular live load of Waegwan is smaller than that of Seonsan. Means of the vehicular live load are calculated with regions and reference lengths by MCS with a million trials and shown in Figure 3.1. Therefore, the statistical model of the vehicular live load is decided adopting data of the vehicular live load of Waegwan.

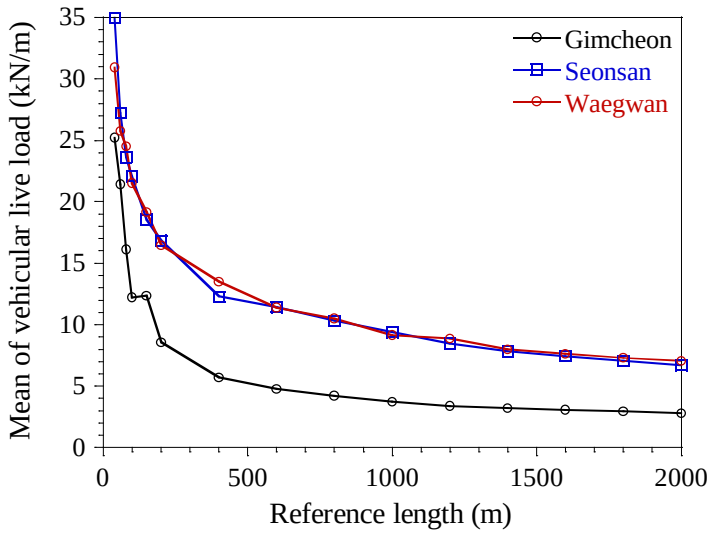

Figure 3.1 Mean of vehicular live load

3.1.3 Distribution Type of Vehicular Live Load

The distribution type of the vehicular live load is verified by the Kolmogorov-Smirnov goodness-of-fit test (K-S test) (Ang and Tang, 2007) with a significance level of 0.01. Candidates of the distribution type are normal, lognormal, Gumbel, and gamma distributions and parameters of each distribution are estimated by the method of moments (Ang and Tang, 2007). The K-S test of each candidate of the distribution type is conducted on the vehicular live load of each reference length. The each K-S test is performed six times through MCS with the sample size from 10^1 to 10^6. The distribution type of the vehicular live load of each reference length is determined with the maximum sample size where at least any distribution type is accepted among candidates of the distribution type. In case several distribution types are not rejected by the K-S tests, the distribution type is decided

as the one having the greatest value of the likelihood function. The likelihood function is defined as follows:

$$L_f(x_1, x_2, \cdots, x_N; \theta_1, \theta_2) = f_X(x_1; \theta_1, \theta_2) f_X(x_2; \theta_1, \theta_2) \cdots f_X(x_N; \theta_1, \theta_2) \quad (3.2)$$

where f_X is the assumed probability density function (PDF) with estimated parameters θ_1 and θ_2 and x_i is an sampling point where the sample size is N. It is simpler to compare natural logarithm of values of likelihood functions:

$$\ln L_f(x_1, x_2, \cdots, x_N; \theta_1, \theta_2) = \sum_{i=1}^{N} \ln f_X(x_i; \theta_1, \theta_2) \quad (3.3)$$

Results of the K-S tests are given in Table 3.3. 'O' indicates that the distribution type is accepted by the K-S test with the maximum sample size. The distribution type of the vehicular live load is confirmed as a Gumbel distribution except for the reference lengths of 40 and 200m. By comparing values of likelihood functions, the distribution type of the vehicular live load is verified as a lognormal and Gumbel distributions for the reference length of 40 and 200m, respectively. The values of natural logarithm of likelihood functions are shown in Table 3.4. The distribution type of the vehicular live load is decided as a Gumbel distribution for all reference lengths in this study because it follows a Gumbel distribution by the K-S tests of most reference lengths.

Table 3.3 Results of K-S tests for the vehicular live load

L (m)	Distribution type				Maximum sample size
	Normal	Lognormal	Gumbel	Gamma	
40	O	O		O	10^3
60			O		10^4
80			O		10^3
100			O		10^3
150			O		10^3
200		O	O	O	10^2
400			O		10^3
600			O		10^3
800			O		10^3
1000			O		10^4
1200			O		10^4
1400			O		10^4
1600			O		10^4
1800			O		10^4
2000			O		10^3

Table 3.4 Values of natural logarithm of likelihood functions for the vehicular live load

L (m)	Distribution type				Maximum sample size
	Normal	Lognormal	Gumbel	Gamma	
40	-1335.7	-1330.8		-1332.3	10^3
200		-190.5	-178.1	-193.3	10^2

3.1.4 Statistical Parameters of Vehicular Live Load

Statistical parameters of the vehicular live load are estimated by the method of least squares. The object function is set to minimize differences between an empirical cumulative distribution function (CDF) and the corresponding theoretical CDF.

$$\mathrm{O} = \frac{1}{2}\sum_{i=1}^{N}\left(\left(F_e\right)_i - F_X\left(x_i;\theta_1,\theta_2\right)\right)^2 \tag{3.4}$$

where $(F_e)_i$ is the empirical CDF of the *i*-th sampling point x_i in ascending order among N samples while F_X is the theoretical CDF with statistical parameters θ_1 and θ_2. By the first-order necessary condition of the object function of Eq. (3.4), the statistical parameters of the vehicular live load are calculated. The sample size is set to 10^6. In case of the vehicular live load, θ_1 and θ_2 are the scale and location parameters, respectively, since it follows a Gumbel distribution.

Values of mean and standard deviation (STD) of the vehicular live load are computed using the statistical parameters by the method of moments and given in Table 3.5. The values of coefficient of variation (COV), which is the ratio of values of STD to mean, are also shown in the table.

Table 3.5 Values of mean, STD, and COV of the vehicular live load

L (m)	Mean	STD	COV
40	31.007	1.013	0.033
60	25.770	1.344	0.052
80	24.436	2.113	0.086
100	21.497	1.511	0.070
150	19.101	1.754	0.092
200	16.386	1.370	0.084
400	13.428	1.301	0.097
600	11.372	0.946	0.083
800	10.482	0.866	0.083
1000	9.159	0.577	0.063
1200	8.894	0.642	0.072
1400	8.005	0.516	0.064
1600	7.653	0.470	0.061
1800	7.306	0.499	0.068
2000	7.071	0.524	0.074

3.2 Design Lane Load

3.2.1 Reference Length

A bridge length in meter which structurally continues is set to the reference length of the design lane load in this study since it is reasonable to load an expected vehicular live load over the bridge length. It could be excessively conservative to consider a loaded length as the reference length.

3.2.2 Design Vehicular Live Load

KL-510, which is the design vehicular live load in the KHBDCs, consists of a design truck in kN and a lane load in kN/m. The design truck is shown in Figure 3.2 and its total load is 510kN. The vehicular live load adopting to design bridges is decided among one of two following cases. The first case is only applying the design truck and the other is to consider the design lane load with 75% of the effect of the design truck. The case causing the greatest response to the cross section of the member being designed is chosen. The design truck makes the maximum effect for short-span bridges and the effect of the design truck is decreasing for longer spans (Nowak *et al*., 2010) so the second case is generally used for long-span bridges. The current design truck is accepted in this study and the design lane load corresponding to the proposed statistical model of the vehicular live load is suggested.

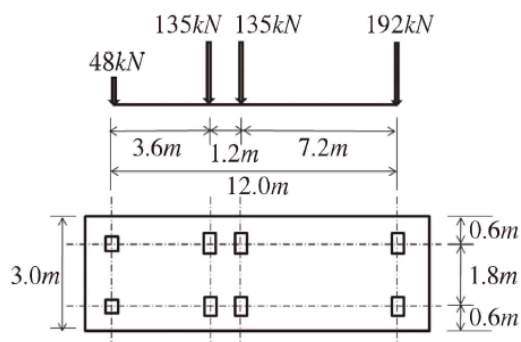

Figure 3.2 Design truck of the KHBDCs (MOLIT, 2016a)

3.2.3 Proposed Design Lane Load

The lane load is calculated by deducting 75% of the effect of the design truck from mean of the vehicular live load where a bridge length is long. For longer spans, the vehicular live load is uniformly distributed (Nowak *et al.*, 2010) so the effect of the design truck is considered as an uniformly distributed load over the reference length. Therefore, the lane load is defined as follows:

$$\tilde{w} = \mu_{LL} - 0.75 \times \left(1.5 \times \frac{510}{L} \right) \tag{3.5}$$

where μ_{LL} is mean of the vehicular live load. The magnitude of the design truck divided by the reference length is multiplied by 1.5 for converting the concentrated load to the distributed load. In case of a simple beam, it is multiplied by 2.0 since the equivalent uniformly distributed load which causes the same moment by the concentrated load is twice greater than the concentrated load divided by the length of the beam. However, the effect of the design truck is conservatively calculated by multiplying 1.5. The lane load is given with the reference length in Figure 3.3.

The design lane load is proposed by drawing an exponential function form of the best-fit-line of the lane load over reference lengths from 100 to 2000m since the lane load is greatest around the reference length of 100m. The proposed design lane load is:

$$w = \begin{cases} 16.5 & (L \le 100) \\ 16.5 \times (100 / L)^{0.28} & (L > 100) \end{cases} \tag{3.6}$$

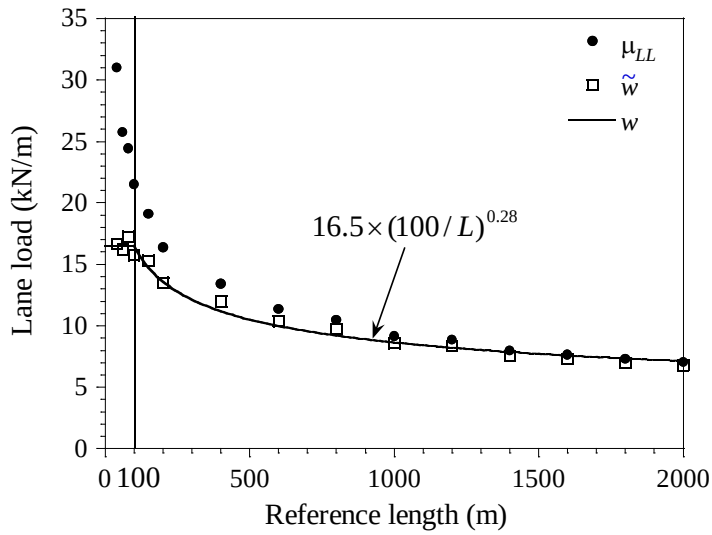

Figure 3.3 Proposed design lane load

The nominal vehicular live load is calculated by adding the effect of the design truck to the proposed design lane load.

The proposed design lane load as well as the design lane load in the KHBDC-C (MOLIT, 2016b) is shown in Figure 3.4 and Table 3.6. The design lane load of the KHBDC is the same with the model 1 of the KHBDC-C (MOLIT, 2016a). The proposed design lane load is less than the design lane load of the KHBDC-C for long-span bridges.

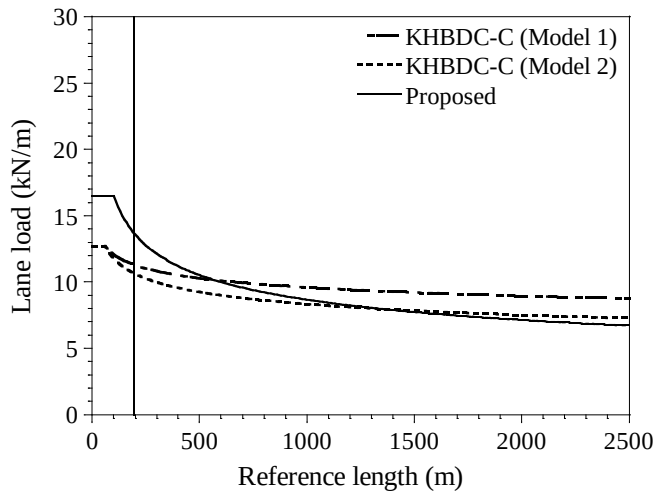

Figure 3.4 Comparison of design lane loads

Table 3.6 Comparison of design lane loads

Design lane load		Magnitude of uniform load (kN/m)	Reference length (m)
KHBDC-C	Model 1	$12.7\times(60/L)^{0.10}$	Span length
	Model 2	$12.7\times(60/L)^{0.15}$	Loaded length
Proposed model		$16.5\times(100/L)^{0.28}$	Structurally continuous bridge length

3.3 Statistical Model of Vehicular Live Load Effect

3.3.1 Formula of Vehicular Live Load Effect

The calculating formula for the statistical model of the vehicular live load effect is proposed by Nowak (1999):

$$Q_{LL} = E \times P \times LL \tag{3.7}$$

where P is the live load analysis factor (an influence factor) for considering uncertainty from the load model which transforms the actual spatially and temporally varying load into a statically equivalent UDL. E is the load analysis factor for taking into account uncertainty from the analysis which transforms the equivalent UDL to a load effect. Statistical parameters of two factors are given in Table 3.7 and it is assumed that the two factors follow a normal distribution. The vehicular live load follow a Gumbel distribution and its statistical parameters are shown in Table 3.5. Statistical characteristics of the vehicular live load effect are decided through MCS and it is assumed that all random variables of Eq. (3.7) are statistically independent each other.

3.3.2 Distribution Type of Vehicular Live Load Effect

A distribution type of the vehicular live load effect is verified by the K-S test with a significance level of 0.01. Candidates of the distribution type are normal, lognormal, Gumbel, and gamma distributions and parameters of each distribution are estimated by the method of moments. The K-S test of each candidate of the distribution type is conducted on the vehicular live load effect of each reference

Table 3.7 Statistical parameters of factors of the formula for the vehicular live load effect (Nowak, 1999)

Factor		Mean	COV
Live load analysis factor	P	1.00	0.12
Load analysis factor	E	1.00	0.06*

* COV for continuous spans

length. The each K-S test is performed six times through MCS with the sample size from 10^1 to 10^6. The distribution type of the vehicular live load effect of each reference length is determined with the maximum sample size where at least any distribution type is accepted among candidates of the distribution type. In case several distribution types are not rejected by the K-S tests, the distribution type is decided as the one having the greatest value of natural logarithm of the likelihood function of Eq. (3.3).

Result of the K-S tests are given in Table 3.8. 'O' indicates that the distribution type is accepted by the K-S test with the maximum sample size. The distribution type of the vehicular live load effect is confirmed as a gamma distribution for all reference lengths but other distributions are not rejected by the K-S tests for some reference lengths. By comparing values of likelihood functions, the distribution types of the vehicular live load effect are verified as gamma distributions for reference lengths of 40, 100, 800, and 2000m while those are confirmed as lognormal distributions for reference lengths of 80, 150, 200, 400, 600, and 1200m. The values of natural logarithm of likelihood functions are shown in Table 3.9. In this study, the distribution type of the vehicular live load effect is decided as a gamma distribution for all reference lengths since distribution types of the vehicular live load effects for nine reference lengths are verified as gamma distributions by the K-S tests and comparison of values of likelihood functions.

Table 3.8 Results of K-S tests for the vehicular live load effect

L (m)	Distribution type				Maximum sample size
	Normal	Lognormal	Gumbel	Gamma	
40	O			O	10^4
60				O	10^5
80		O		O	10^4
100		O		O	10^4
150		O		O	10^4
200		O		O	10^4
400		O		O	10^4
600		O		O	10^4
800		O		O	10^4
1000				O	10^5
1200		O		O	10^4
1400				O	10^5
1600				O	10^5
1800				O	10^5
2000		O		O	10^4

Table 3.9 Values of natural logarithm of likelihood functions for the vehicular live load effect

L (m)	Distribution type				Maximum sample size
	Normal	Lognormal	Gumbel	Gamma	
40	-28669.8			-28649.6	10^4
80		-27610.2		-27617.8	10^4
100		-25967.4		-25954.7	10^4
150		-25443.0		-25449.4	10^4
200		-23608.0		-23608.2	10^4
400		-21946.6		-21966.9	10^4
600		-19966.5		-19976.8	10^4
800		-19153.5		-19147.9	10^4
1200		-17149.3		-17155.9	10^4
2000		-14999.7		-14988.3	10^4

3.3.3 Statistical Parameters of Vehicular Live Load Effect

Statistical parameters of the vehicular live load effect are estimated by the method of least squares. They are calculated by the first-order necessary condition of the object function of Eq. (3.4). The sample size is set to 10^6. In case of the vehicular live load effect, statistical parameters θ_1 and θ_2 of Eq. (3.4) are the shape and scale parameters, respectively, since it follows a gamma distribution.

Values of mean and STD of the vehicular live load effect are computed using the statistical parameters by the method of moments and given in Table 3.10. The

values of COV, nominal, and bias factor, which is the ratio of values of mean to nominal, are also shown in the table. The nominal vehicular live load effect is calculated by Eq. (3.7) where nominal values of the live load analysis and the load analysis factors are set to 1.00 and the nominal vehicular live load is computed by adding the equivalent uniformly distributed load of the design truck to the proposed design lane load.

In Table 3.10, the average of bias factor over reference lengths is 1.00 and the

Table 3.10 Values of mean, STD, COV, nominal, and bias factor of the vehicular live load effect

L (m)	Mean	STD	COV	Nominal	Bias factor
40	31.056	4.295	0.138	30.844	1.007
60	25.792	3.700	0.143	26.063	0.990
80	24.391	3.823	0.157	23.672	1.030
100	21.481	3.221	0.150	22.238	0.966
150	19.052	3.035	0.159	18.554	1.027
200	16.362	2.545	0.156	16.458	0.994
400	13.387	2.165	0.162	12.626	1.060
600	11.357	1.762	0.155	10.947	1.037
800	10.467	1.621	0.155	9.935	1.054
1000	9.158	1.345	0.147	9.233	0.992
1200	8.889	1.338	0.151	8.706	1.021
1400	8.003	1.182	0.148	8.291	0.965
1600	7.653	1.119	0.146	7.950	0.963
1800	7.303	1.088	0.149	7.664	0.953
2000	7.066	1.069	0.151	7.419	0.952

maximum COV is 0.162. Therefore, the bias factor and COV of the vehicular live load effect are decided to 1.00 and 0.17, respectively, for conducting code calibration.

3.3.4 Comparison of Statistical Models of Vehicular Live Load Effect

The current statistical model of the vehicular live load effect follows a lognormal distribution and its bias factor and COV are 1.00 and 0.20, respectively (Lee, 2014). Therefore, it is more variable than the proposed model since the COV of the current model is greater than that of the proposed model. Furthermore, a lognormal distribution is more skewed than a gamma distribution with the same mean μ and STD σ as shown in Figure 3.5.

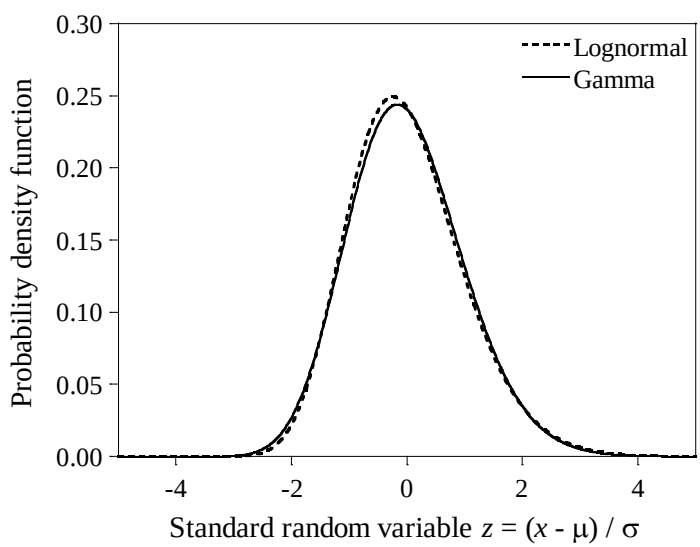

Figure 3.5 PDFs with the same mean and STD

3.4 Multiple Presence Factor

A multiple presence factor is multiplied to the effect induced by the design vehicular live load for considering that the probability which cars exist in several lanes at once is low. Kim (2015) proposed the strategy to calculate multiple presence factors. The principle of the strategy is adopted in this study.

The average of the vehicular live load effect over n lanes is as follows:

$$\mu_{Q_w} = \left(\sum_{i=1}^{n} (Q_w)_i \right) \Big/ n \tag{3.8}$$

where Q_w is the vehicular live load effect of a lane which follows a gamma distribution and its bias factor and COV are 1.00 and 0.17, respectively. Its nominal value is set to 1.00. $(Q_w)_i$ indicates the vehicular live load effect of the *i*-th lane. All vehicular live load effects of a lane are statistically independent and identical. The multiple presence factor of n lanes is defined as in the following:

$$m = \frac{F_2^{-1}(p)}{F_1^{-1}(p)} \tag{3.9}$$

where F_1^{-1} and F_2^{-1} are inverse CDFs of Q_w and μ_{Q_w}, respectively. p is the non-exceedance probability of 0.9999, corresponding to the probability of failure of 10^{-4} for the ULS-1. MCS is conducted with a hundred million trials for computing. The calculated multiple presence factors are given in Table 3.11 and the proposed multiple presence factors as well as multiple presence factors in the

Table 3.11 Calculated multiple presence factors

Number of loaded lanes	1	2	3	4	5	6	7	8
Multiple presence factor	1.00	0.86	0.80	0.77	0.74	0.73	0.71	0.70

KHBDCs (MOLIT, 2016a; MOLIT, 2016b) are shown in Figure 3.6 and Table 3.12. The proposed multiple presence factors are mostly greater than multiple presence factors of the KHBDCs.

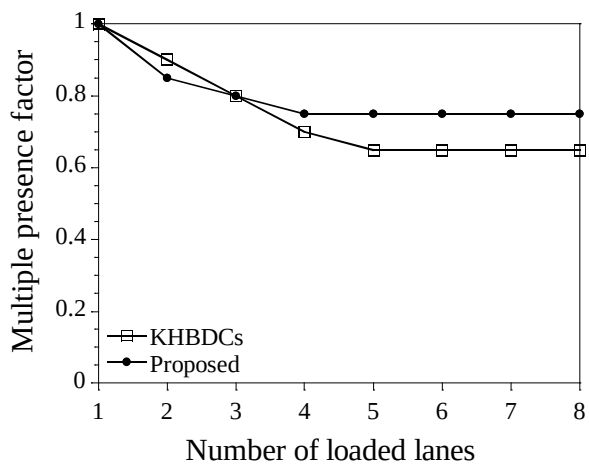

Figure 3.6 Multiple presence factors

Table 3.12 Multiple presence factors

Number of loaded lanes	1	2	3	4	> 5
KHBDCs	1.00	0.90	0.80	0.70	0.65
Proposed	1.00	0.85	0.80	0.75	0.75

This page intentionally left blank

4. CALIBRATION OF ULTIMATE LIMIT STATE I

The calibration is conducted for gravitational loads-governed limit states applying not only the current but also proposed statistical model of the vehicular live load effect by the optimization scheme explained in Chapter 2.

4.1 Gravitational Loads-governed Limit State for KHBDCs

The ULS-I of the KHBDCs mostly consists of dead and vehicular live load effects while the ULS-IV is governed by dead load effects without considering a vehicular live load effect. However, Lee *et al*. (2017) figures out that a vehicular live load effect should be included in the ULS-IV for guaranteeing a uniform level of reliability close to a target reliability index. Therefore, the ULS-I is set as the representative limit state governed by gravitational loads in this study.

4.2 Conditions for Calibration of Ultimate Limit State I

4.2.1 Target Reliability Index, Resistances, and Load Effects for Ultimate Limit State I

The target reliability index for the calibration of the ULS-I is set to 3.72 whose corresponding probability of failure is 10^{-4} since it was applied to determine load factors of the ULS-I for general long-span bridges in the KHBDC-C. In addition,

Table 4.1 Statistical characteristics of resistances

Load effect	Material	Bias factor	COV	Distribution type
Moment	RC	1.229	0.130	Lognormal
	Steel	1.180	0.093	Lognormal
	PC	1.056	0.073	Lognormal
Shear	RC	1.289	0.144	Lognormal
	Steel	1.224	0.115	Lognormal
	PC	1.274	0.139	Lognormal

moment and shear of RC, steel, and PC are adopted as resistances considering major member types in the KHBDCs. Tables 4.1 (Shin *et al.*, 2006; Paik *et al.*, 2009; Bae, 2016) and 4.2 (Nowak, 1999; Lee, 2014) show the statistical characteristics used for reliability analyses. The characteristics of steel members are those of composite steel members given in Table 4.1. In Table 4.2, FM and CIP denote factory-made and cast-in-place members, respectively.

Table 4.2 Statistical characteristics of load effects

Load component		Recurrence period	Bias factor	COV	Distribution type
DC	FM	-	1.03	0.08	Normal
	CIP	-	1.05	0.10	Normal
DW		-	1.00	0.25	Normal
LL	Current	100 yrs	1.00	0.20	Lognormal
	New	100 yrs	1.00	0.17	Gamma

4.2.2 Ranges of DC-dead Load Ratio and Dead Load Ratio

The range of the DC-dead load ratio for the calibration is $0.5 \le \eta \le 1.0$ and Eq. (2.13a) is integrated with respect to the DC-dead load ratio by the left Riemann sum with the integration interval of 0.1.

A range of the dead load ratio in Eq. (2.13a) depends on which set of load factors is optimized and the equation is integrated with respect to the dead load ratio by the 5-point Gauss quadrature with the integration interval of 0.025. The range of the dead load ratio for determination of a set of maximum dead load factors and a vehicular live load factor, for which directions of effects caused by the dead and the vehicular live load are the same, is $0.0 \le \xi \le 1.0$. On the other hand, the ranges of the dead load ratio for which directions of effects induced by the dead and the vehicular live load are opposite are $-5.0 \le \xi \le 0.0$ and $1.0 \le \xi \le 5.0$. The range of $-5.0 \le \xi \le 0.0$ is for obtaining a set of minimum dead load factors while that of $1.0 \le \xi \le 5.0$ is for calculating a minimum live load factor.

The range of the dead load ratio of $0.0 \le \xi \le 1.0$ is split in the three ranges, $0.0 \le \xi \le 0.6$, $0.6 \le \xi \le 0.9$, and $0.9 \le \xi \le 1.0$, for ensuring a uniform level of reliability. The range of $0.0 \le \xi \le 0.6$ is decided based on the dead load ratio of moment in girders of the five existing cable-supported bridges in Korea, the Yi Sun-shin Bridge (YSB), the Ulsan Bridge (UB), the New-millennium Bridge (NMB), the Incheon Bridge (IB), and the Busan Harbor Bridge (BHB). The dead

load ratio calculated applying the model 1 of the design lane load in the KHBDC-C is shown in Figures 4.1(a), 4.1(b), 4.1(c), 4.1(d), and 4.1(e) and that computed using the proposed design lane load is illustrated in Figures 4.2(a), 4.2(b), 4.2(c), 4.2(d), and 4.2(e) (Kim *et al.*, 2017). The dead load ratio in girders mostly exists in the range. Moreover, the range of $0.9 \le \xi \le 1.0$ is decided for load compositions governed by the dead load.

In general, a dead load ratio in girders of short- to medium-span bridges is included in the range of $0.6 \le \xi \le 0.9$ or $0.9 \le \xi \le 1.0$ while that of long-span bridges falls within the range of $0.0 \le \xi \le 0.6$. In addition, a dead load ratio in cables of long-span bridges is covered by the range of $0.6 \le \xi \le 0.9$ or $0.9 \le \xi \le 1.0$.

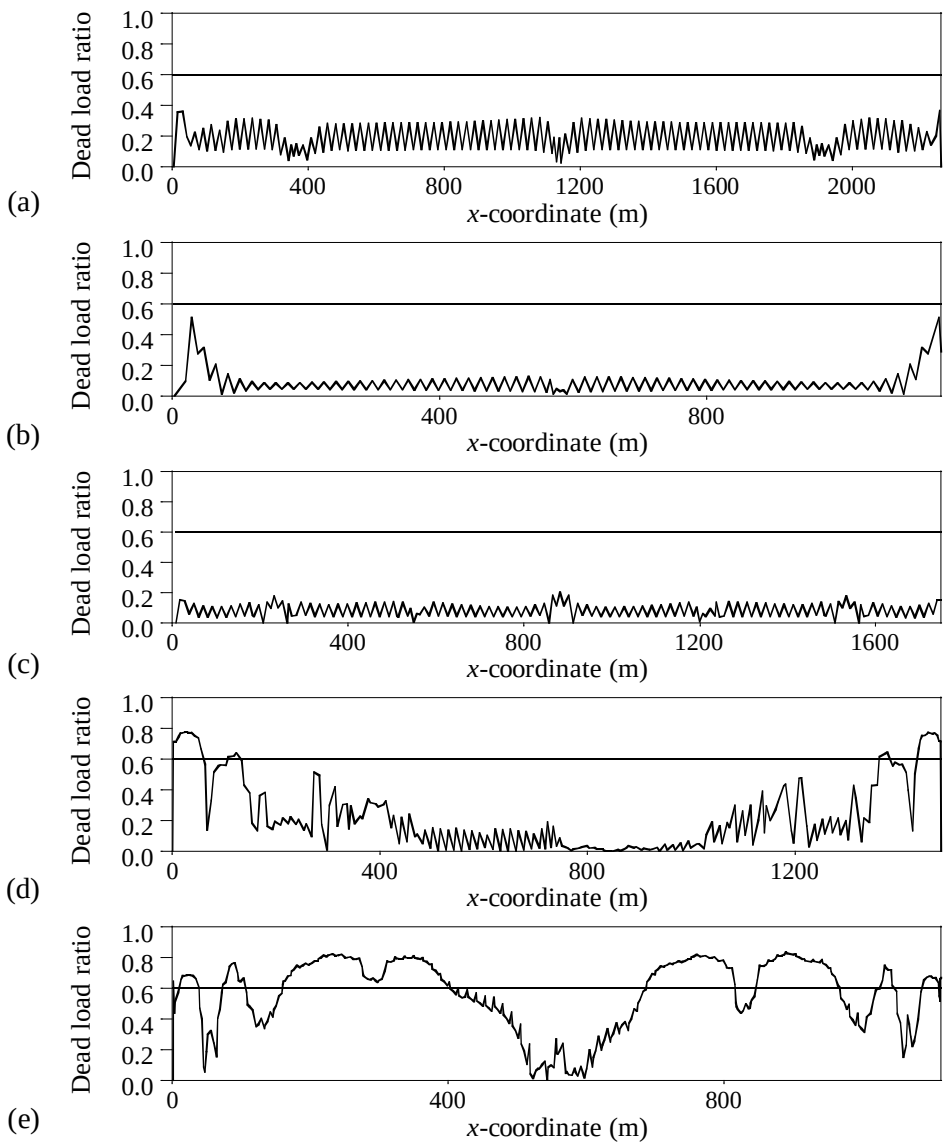

Figure 4.1 The dead load ratio of moment in girders of the five existing cable-supported bridges in Korea with the *x*-coordinate, which is the longitudinal direction of the bridge, by applying the model 1 of the design lane load in the KHBDC-C: (a) YSB, (b) UB, (c) NMB, (d) IB, (e) BHB

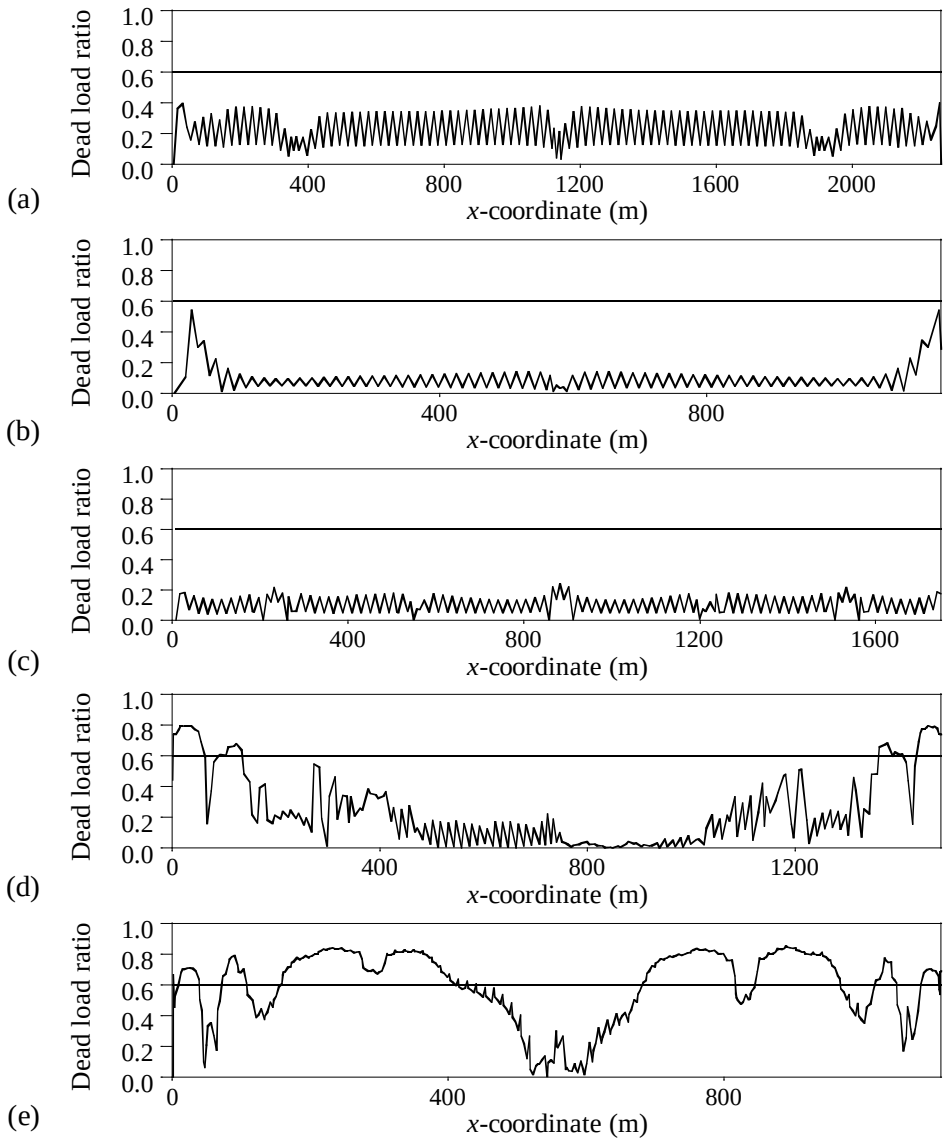

Figure 4.2 The dead load ratio of moment in girders of the five existing cable-supported bridges in Korea with the *x*-coordinate, which is the longitudinal direction of the bridge, by applying the proposed design lane load: (a) YSB, (b) UB, (c) NMB, (d) IB, (e) BHB

4.3 Determination of L-R Factors for Ultimate Limit State I

4.3.1 Calibration Process of Ultimate Limit State I

Load factors are proposed depending on the range of a dead load ratio, by which any type of a bridge could be designed. Therefore, optimizations for calculating the load factors in each of ranges are separately conducted with respect to the ranges while the resistance factors are consistent over the ranges.

Firstly, the resistance factors for moment of RC, steel, and PC and the load factors of *DC*, *DW*, and *LL* for the range of $0.6 \le \xi \le 0.9$ are computed by the optimization with respect to the range of $0.6 \le \xi \le 0.9$. The resistance factor of RC for moment is fixed at 0.90, which is the equivalent resistance factor to the corresponding material factor in the KHBDCs (Bae, 2016), to get the unique solution of L-R factors in the optimization. The resistance factors for shear of RC, steel, and PC are calculated by the optimization with holding the proposed load factors for the range of $0.6 \le \xi \le 0.9$.

In addition, the load factors of *DC*, *DW*, and *LL* are optimized for the ranges of $0.0 \le \xi \le 0.6$ and $0.9 \le \xi \le 1.0$ separately by fixing the suggested resistance factors for moment. Also, the load factors of *DC* and *DW* for the range of $-5.0 \le \xi \le 0.0$ are computed by the optimization conducted to apply the proposed resistance factors for moment and the suggested load factor of *LL* for the range of $0.0 \le \xi \le 0.6$ considering continuity of load factors. On the other hand, the load

factor of *LL* for the range of $1.0 \le \xi \le 5.0$ is calculated by the optimization performed to hold the proposed resistance factors for moment and the suggested load factors of *DC* for factory-made members and *DW* for the range of $0.9 \le \xi \le 1.0$ taking into account continuity of load factors.

In each range of a dead load ratio except the range of $1.0 \le \xi \le 5.0$, optimizations are carried out twice to determine load factors. The first optimization is conducted for a set of load factors with a load factor of *DC* for factory-made members and the second optimization is performed for a load factor of *DC* for cast-in-place members by fixing the suggested load factors for *DW* and *LL* of the first optimization.

The proposed values of the resistance factors are determined by rounding off the calculated values of the resistance factors to the second decimal point since the reliability index decreases by about 0.9 while the resistance factor increases by 0.1 (Lee *et al.*, 2017). In addition, the suggested values of the load factors in the range of $0.0 \le \xi \le 0.6$, $0.6 \le \xi \le 0.9$, and $0.9 \le \xi \le 1.0$ are decided where the average of the reliability index over DC-dead load ratios, member types, and dead load ratios applying the proposed L-R factors satisfies the target reliability index the most closely. The proposed values of the load factors in the ranges of $-5.0 \le \xi \le 0.0$ and $1.0 \le \xi \le 5.0$, on the other hand, are determined where the average of the reliability index over DC-dead load ratios and member types using the suggested L-R factors assures the target reliability index over the range.

4.3.2 Proposed L-R Factors for Ultimate Limit State I

Two calibrations of the ULS-1 are conducted applying the current and the new statistical models of the vehicular live load effect, respectively. The calculated and proposed values of the L-R factors by the optimizations are given in Tables 4.3 and 4.4 with the L-R factors in the KHBDCs (MOLIT, 2016a; MOLIT, 2016b). Opt. and Prop. denote the optimized and the proposed values, respectively, and the Current Q_{LL} and the New Q_{LL} indicate the results of optimizations adopting the current and the new statistical models of the vehicular live load effect, respectively. Since the KHBDCs adopt material factors, the equivalent resistance factors of RC and PC for moment and shear to the material factors are given in Table 4.3 (Bae, 2016). Also, the load factors for the ULS-IV of the KHBDCs are given in the parentheses in Table 4.4 because the ULS-I and IV are split at $\xi = 0.875$ in the KHBDC and $\xi = 0.95$ in the KHBDC-C, respectively.

Table 4.3 The current, optimized, and proposed resistance factors

Load effect	Material	KHBDCs	Current Q_{LL}		New Q_{LL}	
			Opt.	Prop.	Opt.	Prop.
Moment	RC	0.90*	0.900	0.90	0.900	0.90
	Steel	1.00	0.967	0.97	0.971	0.97
	PC	0.90*	0.914	0.91	0.920	0.92
Shear	RC	0.90*	0.906	0.91	0.906	0.91
	Steel	1.00	0.944	0.94	0.947	0.95
	PC	0.90*	0.911	0.91	0.911	0.91

* Equivalent resistance factors to material factors

Table 4.4 The current, optimized, and proposed load factors for the ULS-I

Dead load ratio	Load factor		KHBDC	KHBDC-C	Current Q_{LL}		New Q_{LL}	
					Opt.	Prop.	Opt.	Prop.
$-5.0 \le \xi \le 0.0$	γ_{DC}	FM	0.90	0.85	0.936	0.85	0.975	0.90
		CIP		0.85	0.973	0.85	0.985	0.90
	γ_{DW}		0.65	0.80	0.826	0.75	0.816	0.80
	γ_{LL}		1.80	1.80	1.800	1.80	1.600	1.60
$0.0 \le \xi \le 0.6$	γ_{DC}	FM	1.25	1.15	1.047	1.05	1.100	1.10
		CIP		1.20	1.069	1.10	1.130	1.15
	γ_{DW}		1.50	1.25	1.131	1.15	1.217	1.20
	γ_{LL}		1.80	1.80	1.797	1.80	1.591	1.60
$0.6 \le \xi \le 0.9$	γ_{DC}	FM	1.25 (1.50)	1.15	1.222	1.20	1.244	1.25
		CIP		1.20	1.245	1.25	1.292	1.30
	γ_{DW}		1.50 (1.50)	1.25	1.463	1.50	1.499	1.50
	γ_{LL}		1.80 (N/A)	1.80	1.459	1.50	1.332	1.35
$0.9 \le \xi \le 1.0$ *	γ_{DC}	FM	(1.50)	1.15 (1.25)	1.258	1.25	1.264	1.30
		CIP		1.20 (1.25)	1.310	1.30	1.333	1.35
	γ_{DW}		(1.50)	1.25 (1.35)	1.562	1.60	1.569	1.55
	γ_{LL}		(N/A)	1.80 (N/A)	1.112	1.10	1.112	1.15
$1.0 \le \xi \le 5.0$	γ_{DC}	FM	(N/A)	(N/A)	1.250	1.25	1.300	1.30
		CIP	(N/A)	(N/A)	-	1.30	-	1.35
	γ_{DW}		(N/A)	(N/A)	1.600	1.60	1.550	1.55
	γ_{LL}		(N/A)	(N/A)	0.803	0.75	0.861	0.80

* The values in the parentheses are the load factors for the ULS-IV

In Table 4.3, the resistance factors proposed by the optimizations are similar to those in the KHBDCs. The differences between the resistance factors of the KHBDCs and the proposed values are up to 6% and 5% for the current and the new statistical models of the vehicular live load effect, respectively. In case of the current model, the load factor of *LL* suggested in the range of $0.0 \le \xi \le 0.6$ where the vehicular live load governs the limit state is, furthermore, the same with that of the KHBDC or the KHBDC-C shown in Table 4.4. The load factors of *DC* and *DW* proposed in the range of $0.6 \le \xi \le 0.9$, within which a dead load ratio in girders of short- to medium-span bridges falls, are equal to those of the KHBDC. In the range of $-5.0 \le \xi \le 0.0$, the proposed load factors of *DC* are coincident with those of the KHBDC-C.

Compared to load factors by the current and new statistical models of the live load effect, the load factors of *LL* by the new statistical model are mostly less than those by the current one while the load factors of *DC* and *DW* are in reverse because the current statistical model is more skewed and variable than the new one. Moreover, Figure 4.3 shows that the factored land load of the new model, which is the proposed design lane load multiplied by the suggested load factor of *LL* by the new model, is less than that of the current model, which is the model 1 of the design lane load in the KHBDC-C multiplied by the proposed load factor of *LL* by the current model, for long reference lengths.

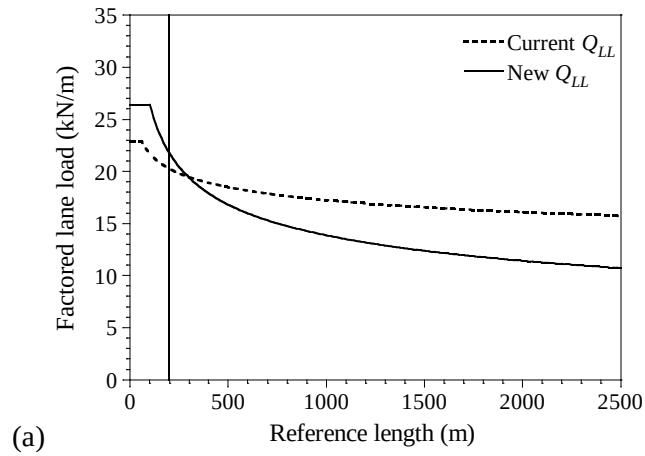

(a)

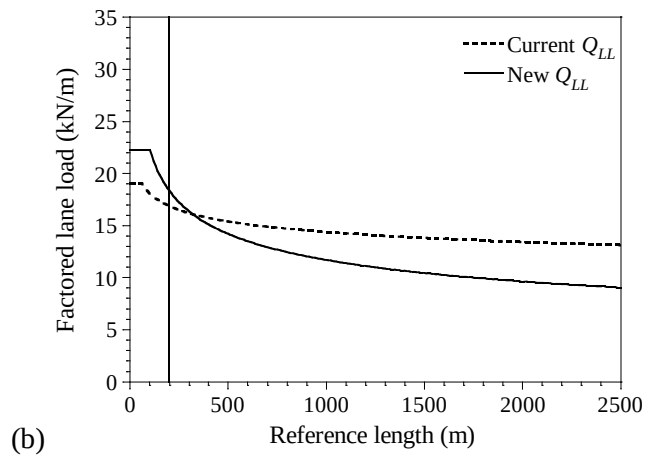

(b)

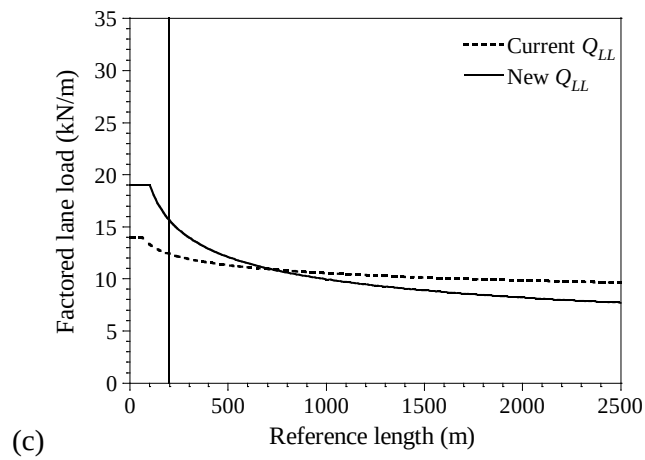

(c)

Figure 4.3 Comparison of factored lane load: (a) $0.0 \le \xi \le 0.6$, (b) $0.6 \le \xi \le 0.9$, (c) $0.9 \le \xi \le 1.0$

4.3.3 Results of Reliability Analyses by Proposed L-R Factors of Ultimate Limit State I

Figures 4.4 and 4.5 show the variation of the reliability index for moment with the dead load ratio of $0.0 \le \xi \le 1.0$ for five DC-dead load ratios adopting the proposed L-R factors by the current and the new statistical models of the vehicular live load effect, respectively, with the load factors of *DC* for factory-made members. The DC-dead load ratios are the left-end points, 0.5, 0.6, 0.7, 0.8, and, 0.9, for the integration of Eq. (2.13a) by the left Riemann sum. Figures 4.6 and 4.7 present the variation of the reliability index for moment with the dead load ratio of $-5.0 \le \xi \le 0.0$ and $1.0 \le \xi \le 5.0$, respectively, for five DC-dead load ratios using applying the suggested L-R factors by the current model.

In addition, Figures from 4.8 to 4.12 illustrate the average reliability index over the five DC-dead load ratios for three member types. In case of the current statistical model of the vehicular live load effect, the maximum error of the average reliability index to the target reliability index is 5.1% in the range of $0.0 \le \xi \le 1.0$ while it is 10.9% in the range of $-5.0 \le \xi \le 0.0$ and $1.0 \le \xi \le 5.0$ since the criteria for determining the load factors are different. On the other hand, the maximum error of the average reliability index to the target reliability index is 4.6% in the range of $0.0 \le \xi \le 1.0$ while it is 12.8% in the ranges of $-5.0 \le \xi \le 0.0$ and $1.0 \le \xi \le 5.0$ in case of the new statistical model.

The average of the reliability index over the five DC-dead load ratios and three

member types is plotted in Figures 4.13(a) and (b). In the range of $0.0 \le \xi \le 1.0$, it satisfies the target reliability index over the range within ± 4% error bounds to the target reliability index where the proposed L-R factors are applied, whereas it is greater than the target reliability index with up to a 22% error to the target reliability index where the L-R factors of the KHBDC are used. The average of the reliability index over the five DC-dead load ratios and three member types adopting the L-R factors of the KHBDC-C, moreover, is less than the target reliability index with a negative error of 23% to the target reliability index in the dead load-governed range. Nevertheless, the load factors of the KHBDC-C is applicable in the range of $0.0 \le \xi \le 0.8$ because the average reliability index is included in the ± 6% error bounds of the target reliability index in the range. In the range of $-5.0 \le \xi \le 0.0$, the proposed L-R factors, meanwhile, assures the target reliability index within a 5% error to the target reliability index which is similar to the reliability level of the KHBDC and the KHBDC-C.

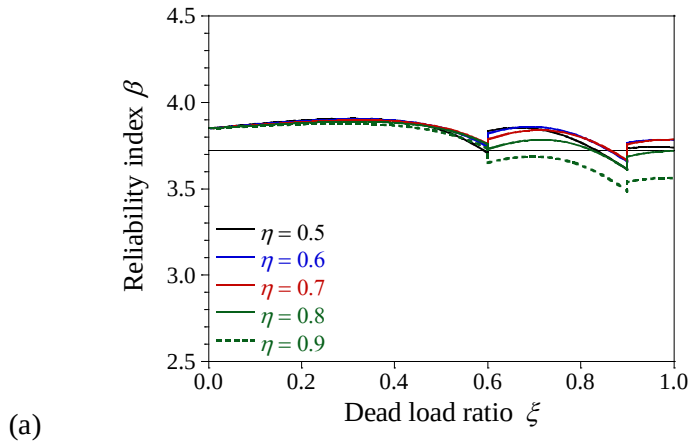

(a)

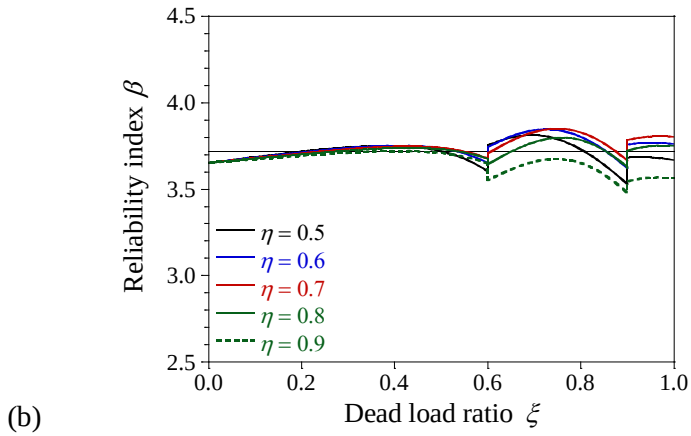

(b)

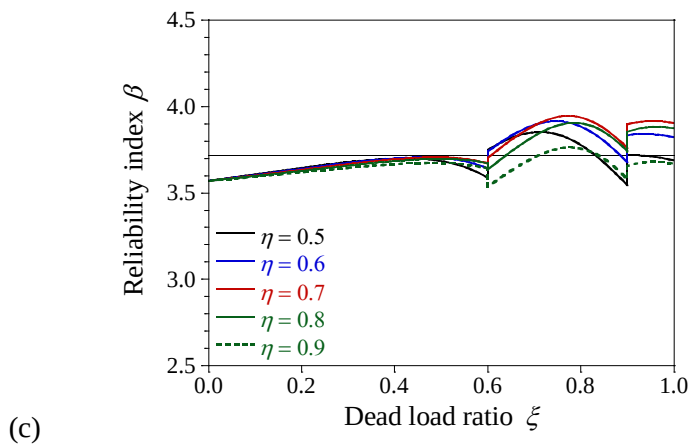

(c)

Figure 4.4 Variation of the reliability index for moment with the dead load ratio of $0.0 \le \xi \le 1.0$ applying the proposed L-R factors by the current statistical model of the vehicular live load effect with the load factors of *DC* for factory-made members: (a) RC, (b) Steel, (c) PC

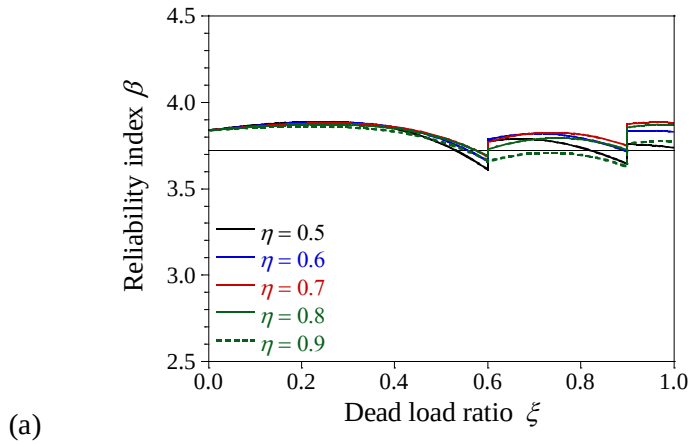

(a)

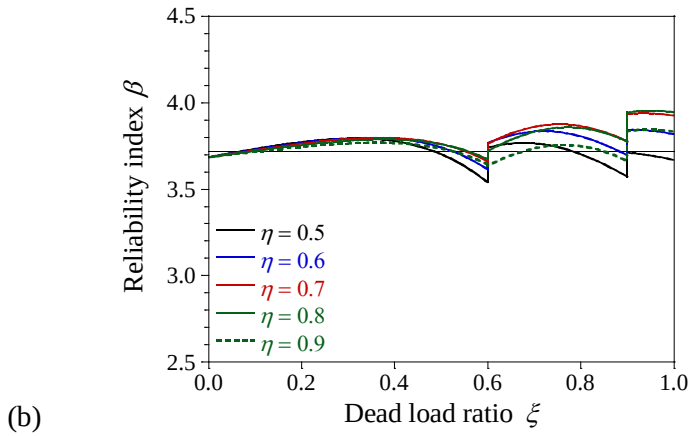

(b)

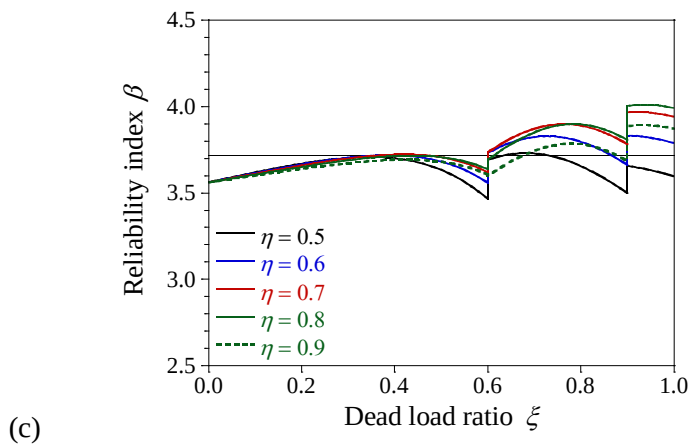

(c)

Figure 4.5 Variation of the reliability index for moment with the dead load ratio of $0.0 \le \xi \le 1.0$ applying the proposed L-R factors by the new statistical model of the vehicular live load effect with the load factors of *DC* for factory-made members: (a) RC, (b) Steel, (c) PC

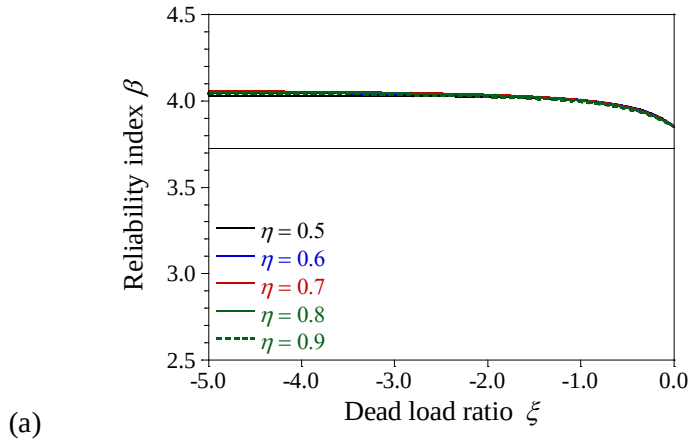

(a)

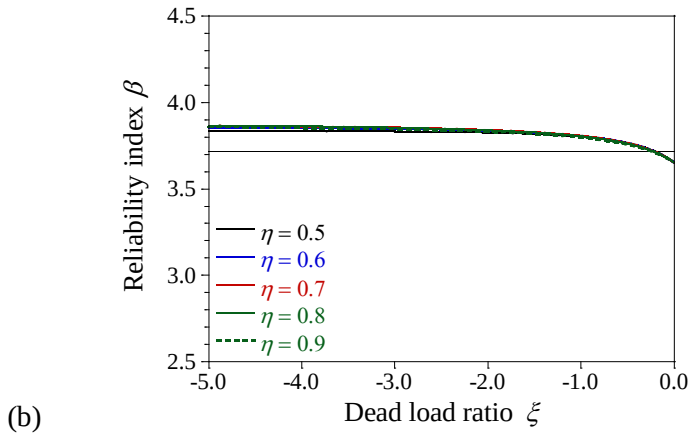

(b)

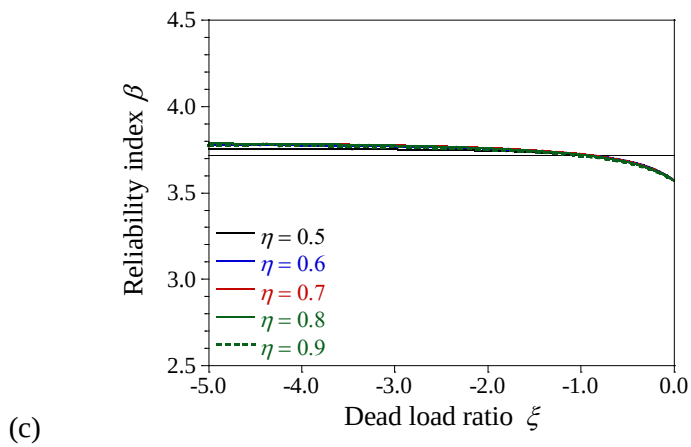

(c)

Figure 4.6 Variation of the reliability index for moment with the dead load ratio of $-5.0 \le \xi \le 0.0$ applying the proposed L-R factors by the current statistical model of the vehicular live load effect with the load factors of *DC* for factory-made members: (a) RC, (b) Steel, (c) PC

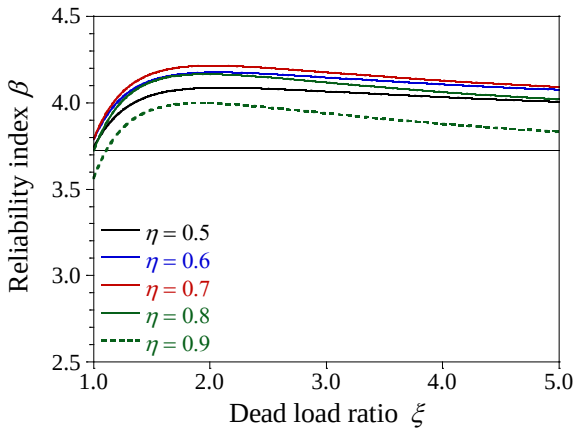

(a)

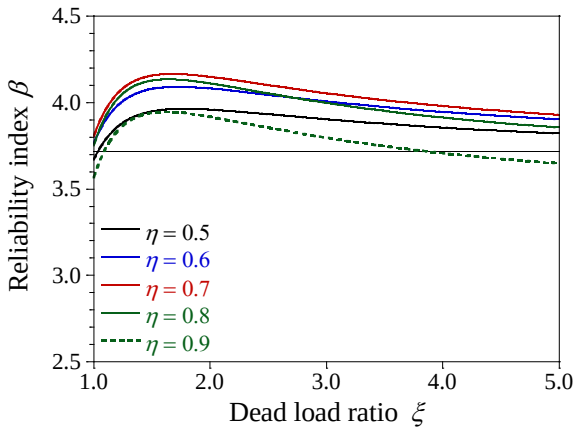

(b)

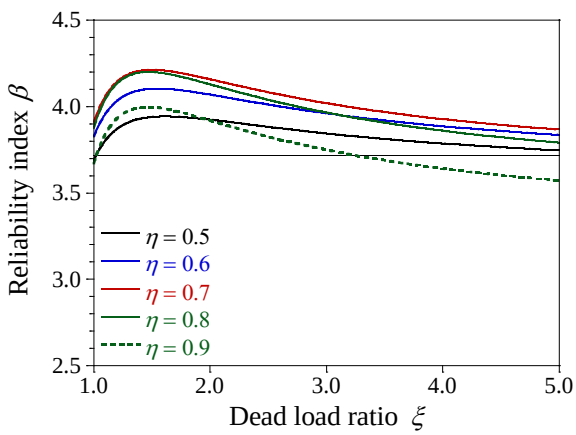

(c)

Figure 4.7 Variation of the reliability index for moment with the dead load ratio of $1.0 \le \xi \le 5.0$ applying the proposed L-R factors by the current statistical model of the vehicular live load effect with the load factors of *DC* for factory-made members: (a) RC, (b) Steel, (c) PC

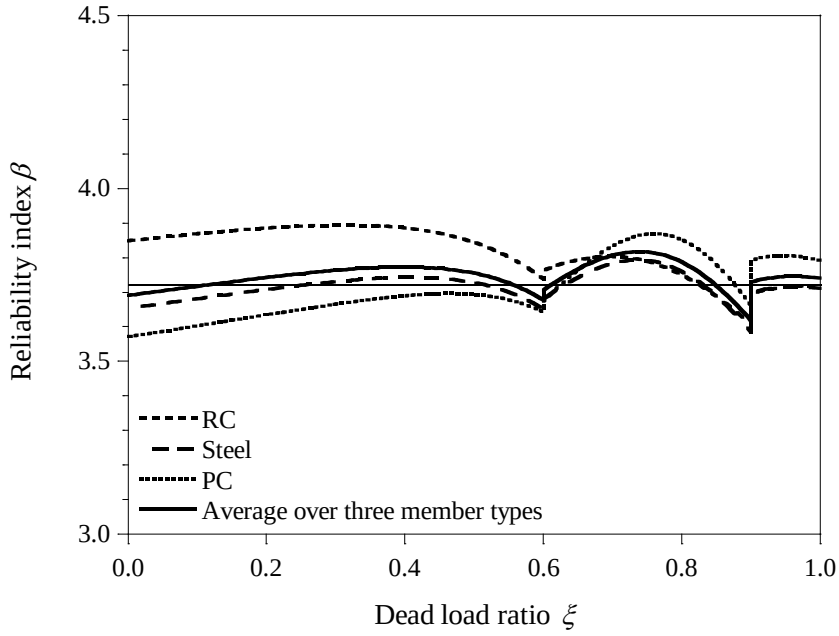

(a)

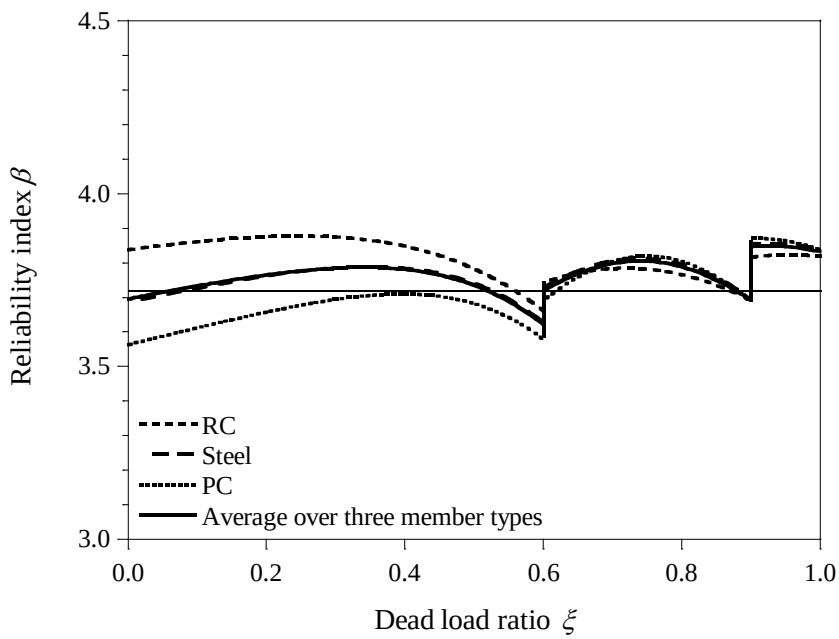

(b)

Figure 4.8 Variation of the average reliability index for moment over five DC-dead load ratios with the dead load ratio of $0.0 \le \xi \le 1.0$ applying the proposed L-R factors with the load factors of *DC* for factory-made members: (a) By the current model, (b) By the new model

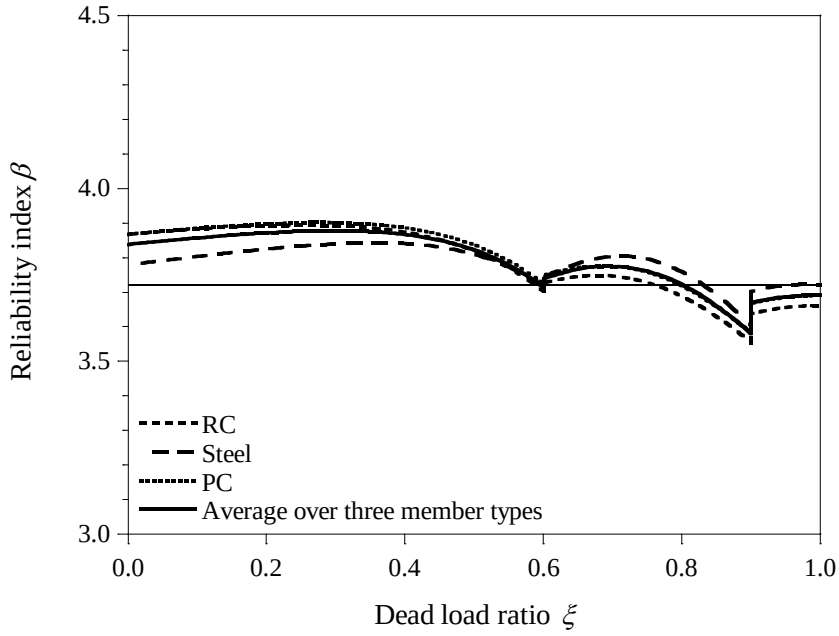

(a)

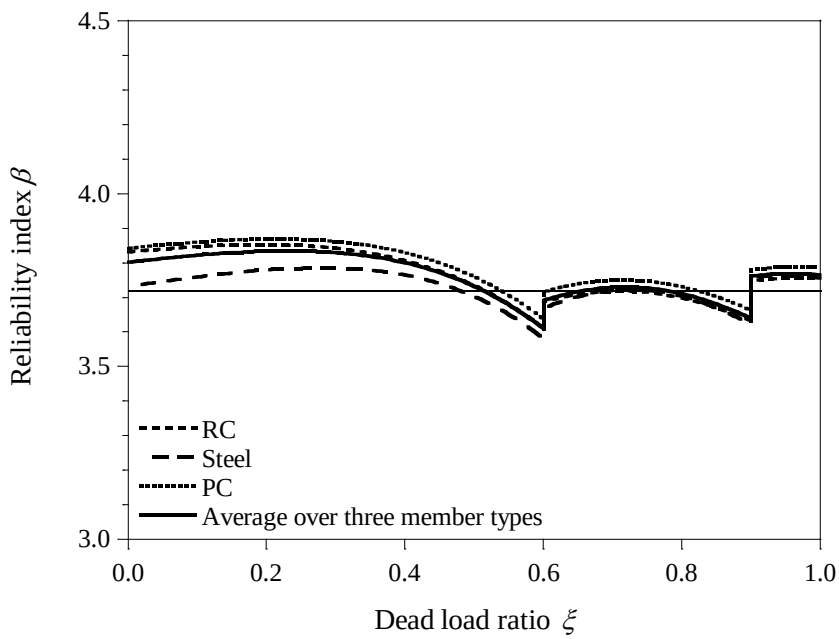

(b)

Figure 4.9 Variation of the average reliability index for shear over five DC-dead load ratios with the dead load ratio of $0.0 \le \xi \le 1.0$ applying the proposed L-R factors with the load factors of *DC* for factory-made members: (a) By the current model, (b) By the new model

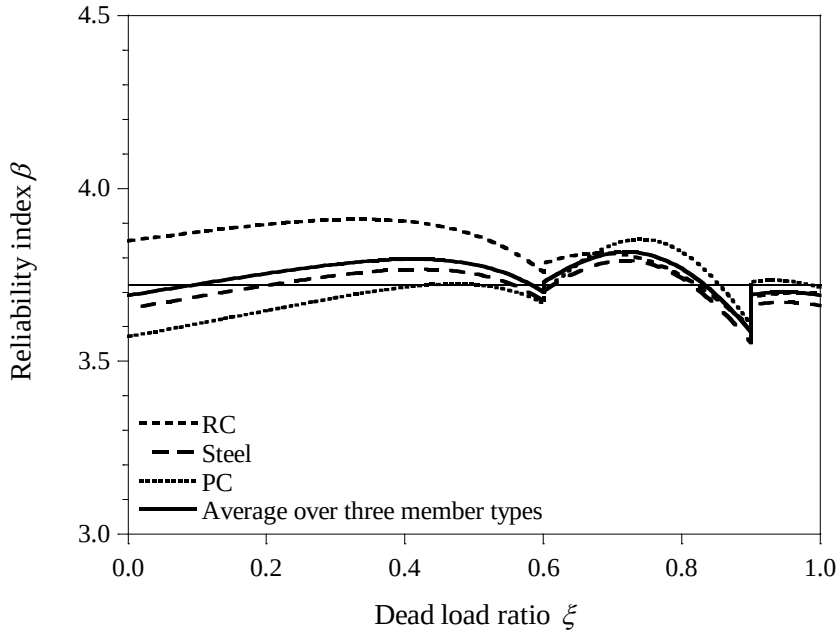

(a)

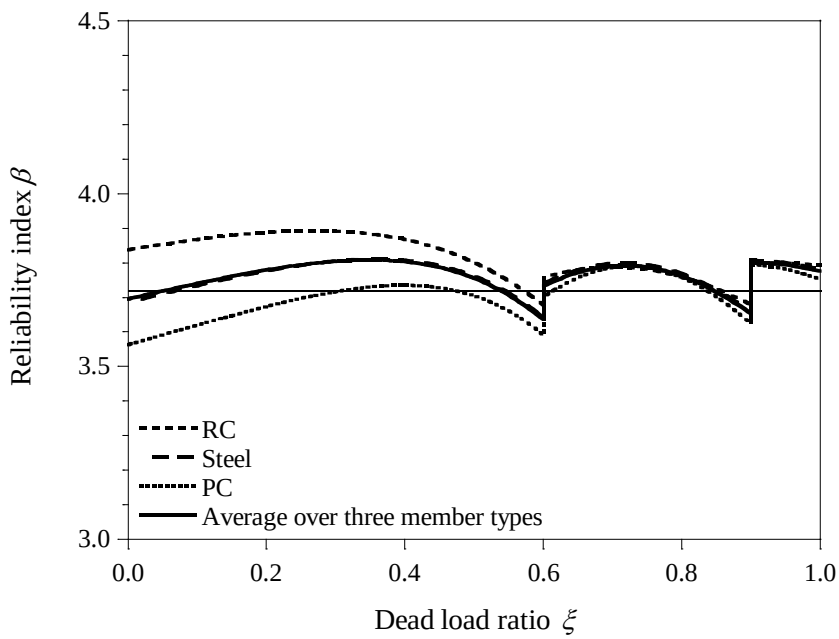

(b)

Figure 4.10 Variation of the average reliability index for moment over five DC-dead load ratios with the dead load ratio of $0.0 \le \xi \le 1.0$ applying the proposed L-R factors with the load factors of *DC* for cast-in-place members: (a) By the current model, (b) By the new model

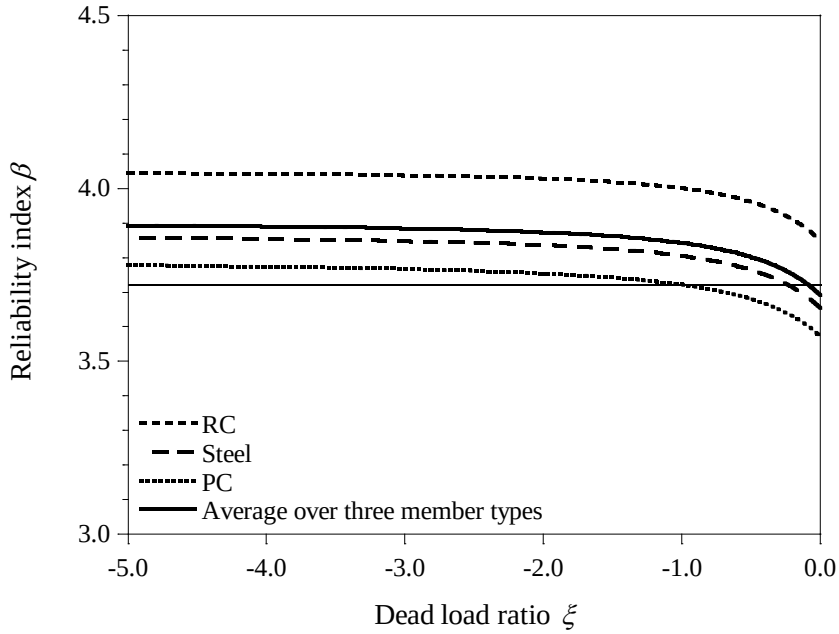

(a)

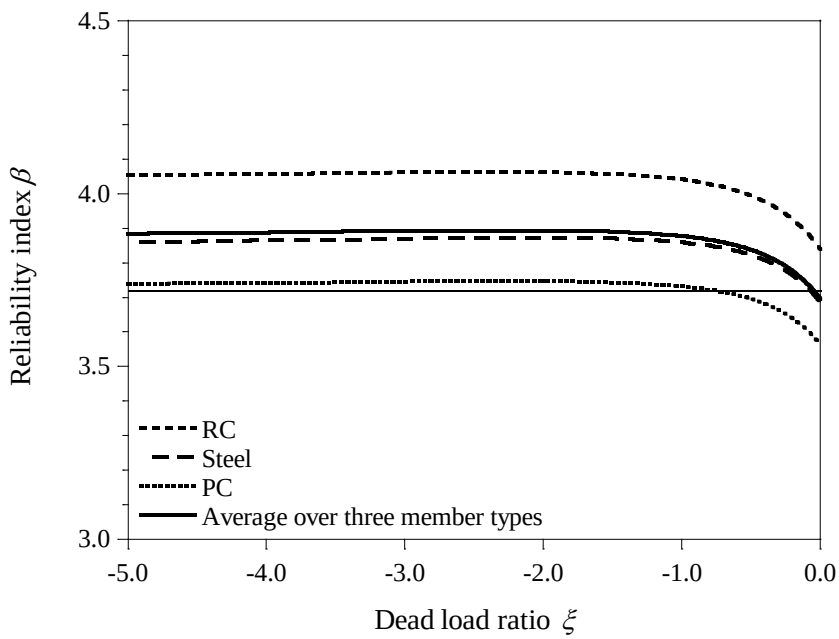

(b)

Figure 4.11 Variation of the average reliability index for moment over five DC-dead load ratios with the dead load ratio of $-5.0 \le \xi \le 0.0$ applying the proposed L-R factors with the load factors of *DC* for factory-made members: (a) By the current model, (b) By the new model

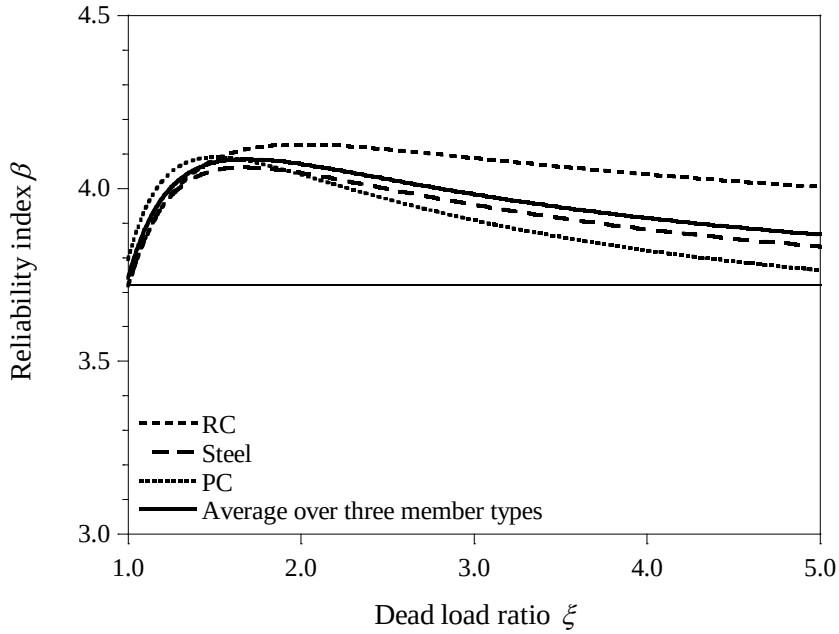

(a)

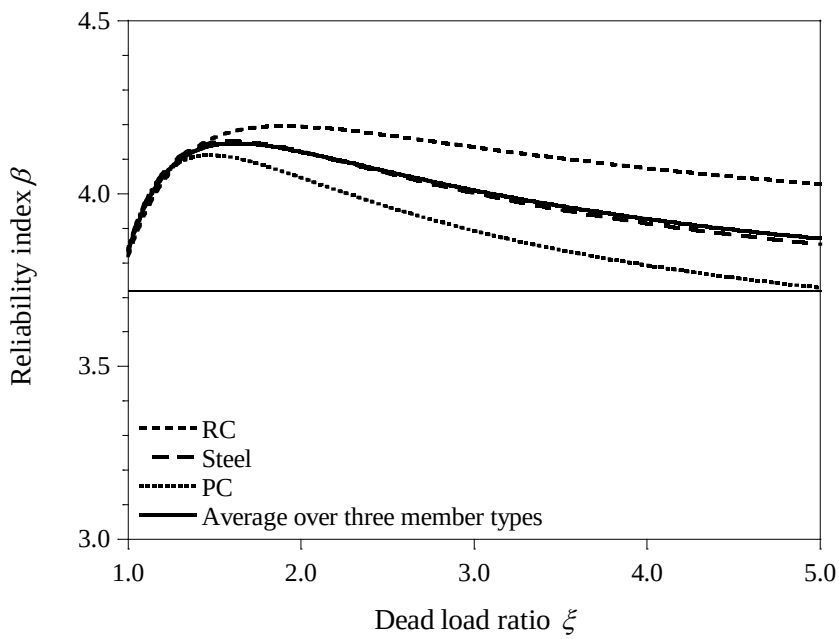

(b)

Figure 4.12 Variation of the average of the reliability index for moment over five DC-dead load ratios with the dead load ratio of $1.0 \le \xi \le 5.0$ applying the proposed L-R factors with the load factors of *DC* for factory-made members: (a) By the current model, (b) By the new model

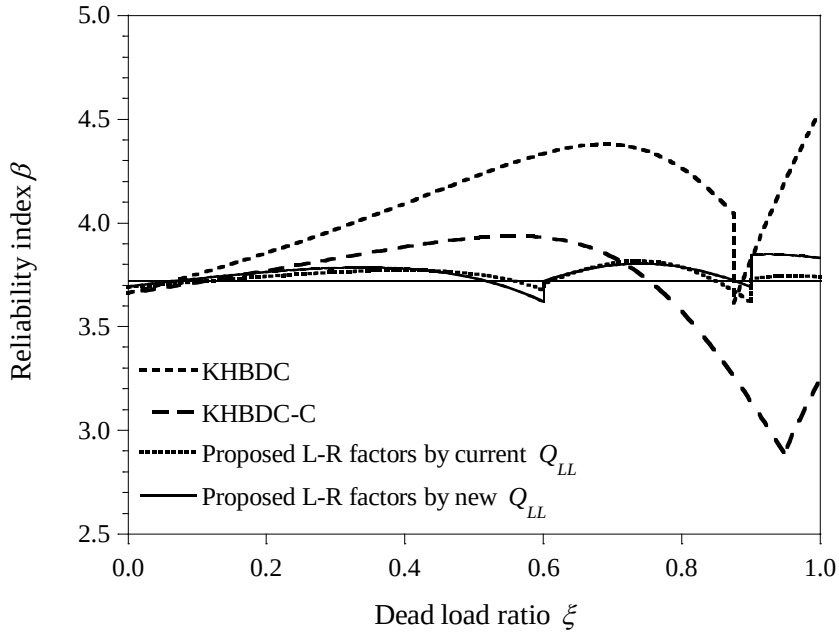

(a)

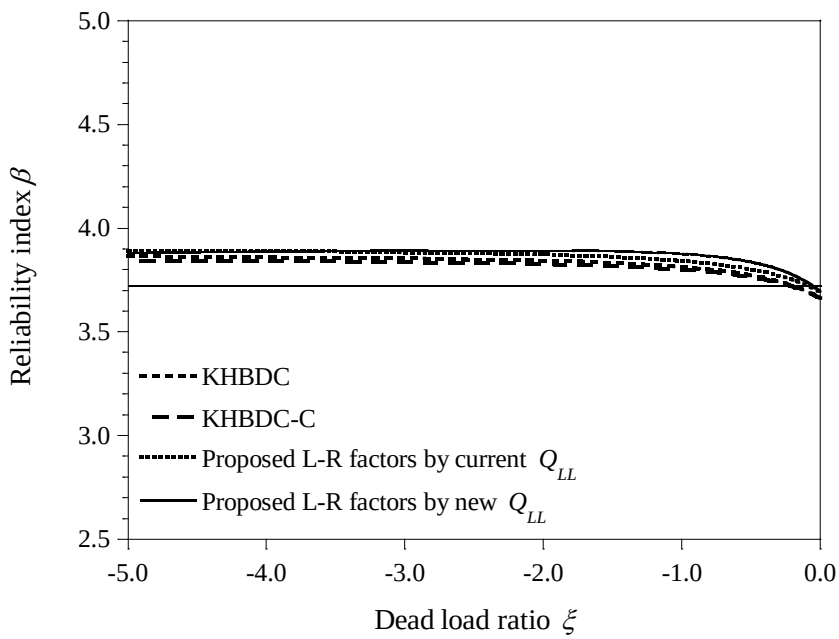

(b)

Figure 4.13 Variation of the average reliability index for moment over the five DC-dead load ratios and the three member types with the dead load ratio applying the current and proposed L-R factors with the load factors of *DC* for factory-made members: (a) In the range of $0.0 \le \xi \le 1.0$, (b) In the range of $-5.0 \le \xi \le 0.0$

4.3.4 Additional Proposal of Load Factors

The proposed load factors are defined in the three ranges of the dead load ratio, where directions of effects induced by the dead and the vehicular live loads are the same, for assuring a uniform level of reliability. Moreover, it is split in the two ranges, $0.6 \le \xi \le 0.9$ and $0.9 \le \xi \le 1.0$, where the limit state is governed by the dead load. However, it might be complex to adopt the suggested sets of load factors in design codes. Therefore, a set of load factors in the integrated range of the dead load ratio, $0.6 \le \xi \le 1.0$, is additionally proposed in this study.

The load factors of *DC*, *DW*, and *LL* are computed for the range of $0.6 \le \xi \le 1.0$ by fixing the suggested resistance factors for moment, shown in Table 4.3. The calculated and proposed values of the load factors in the integrated range of $0.6 \le \xi \le 1.0$ are given in Table 4.5.

Figures 4.14(a) and (b) show the average reliability index over the five DC-

Table 4.5 The current, optimized, and proposed load factors for the ULS-I in the integrated range of $0.6 \le \xi \le 1.0$

Dead load ratio	Load factor		KHBDC	KHBDC-C	Current Q_{LL}		New Q_{LL}	
					Opt.	Prop.	Opt.	Prop.
$0.6 \le \xi \le 1.0$ *	γ_{DC}	FM	1.25 (1.50)	1.15 (1.25)	1.244	1.25	1.257	1.25
		CIP		1.20 (1.25)	1.299	1.30	1.305	1.30
	γ_{DW}		1.50 (1.50)	1.25 (1.35)	1.508	1.50	1.529	1.55
	γ_{LL}		1.80 (N/A)	1.80 (N/A)	1.378	1.40	1.284	1.30

* The values in the parentheses are the load factors for the ULS-IV

dead load ratios for three member types. The maximum errors of the reliability index to the target reliability index by the current and the new models are 5.2% and 3.2% in the range of $0.6 \le \xi \le 1.0$ while those are both 4.0% in the range in Figures 4.8(a) and (b). The averages of the reliability index over the five DC-dead load ratios and three member types by the current and the new models are plotted in Figure 4.15. In the range of $0.6 \le \xi \le 1.0$, those are included in the ± 4% and ± 3% error bounds of the target reliability index, respectively, whereas those exist in the ± 3% and ± 4% error bounds of the target reliability index in Figure 4.13(a). Therefore, it is allowable to adopt the set of load factors in the integrated range of $0.6 \le \xi \le 1.0$ in lieu of the sets of load factors in the ranges of $0.6 \le \xi \le 0.9$ and $0.9 \le \xi \le 1.0$.

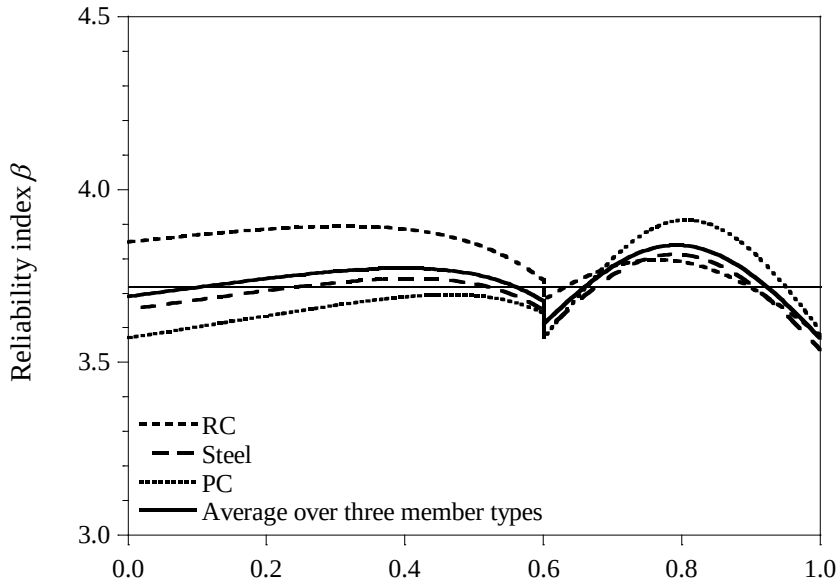

(a)

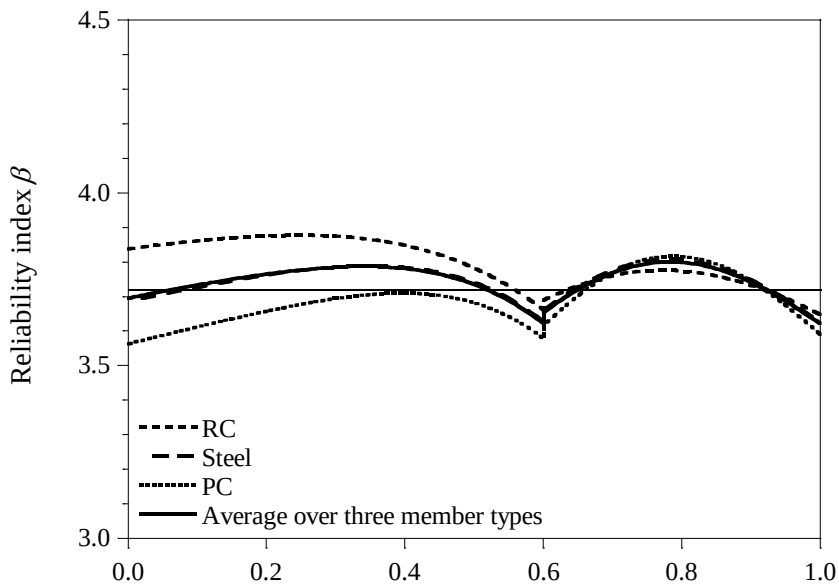

(b)

Figure 4.14 Variation of the average reliability index for moment over five DC-dead load ratios with the dead load ratio of $0.0 \le \xi \le 1.0$ applying the proposed L-R factors with the load factors of *DC* for factory-made members and the load factors in the integrated range of $0.6 \le \xi \le 1.0$: (a) By the current model, (b) By the new model

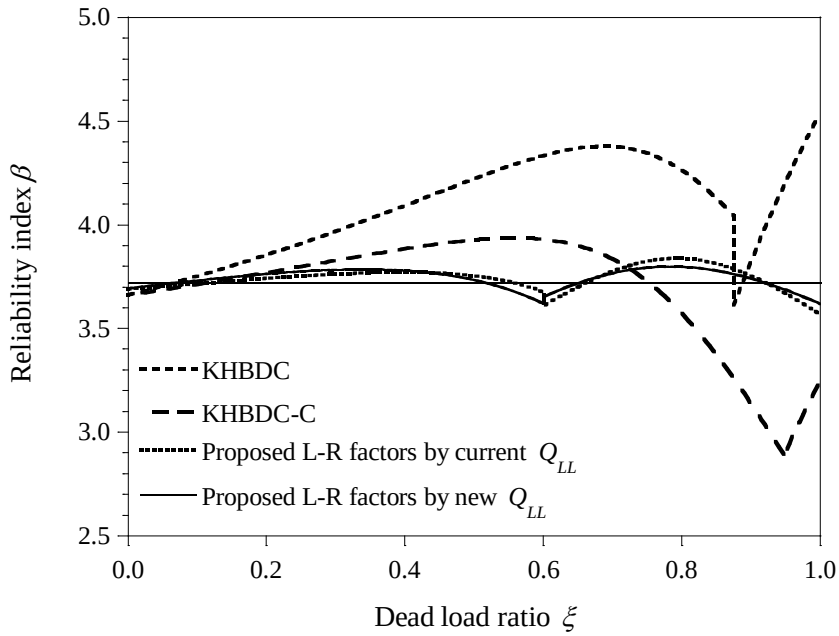

Figure 4.15 Variation of the average reliability index for moment over five DC-dead load ratios and the three member types with the dead load ratio of $0 \le \xi \le 1.0$ applying the current and proposed L-R factors with the load factors of *DC* for factory-made members and the load factors in the integrated range of $0.6 \le \xi \le 1.0$

5. CALIBRATION OF ULTIMATE LIMIT STATE V

The calibration is conducted for the ULS-V, whose major components are dead, vehicular live, and wind load effects, applying not only the current but also proposed statistical model of the vehicular live load effect by the optimization scheme explained in Chapter 2. The statistical characteristics of the wind load effect induced by the wind velocity of 25m/s are decided for short- to medium-span and long-span bridges, separately, to conduct the calibration.

5.1 Statistical Model of Wind Load Effect Induced by Wind Velocity of 25m/s

5.1.1 Formula of Wind Load Effect Induced by Wind Velocity of 25m/s

The calculating formula for the statistical model of the wind load effect induced by the wind velocity of 25m/s is proposed by Ellingwood *et al*. (1980):

$$Q_{WS_{25}} = cC_pE_ZGV_{25}^2 \tag{5.1}$$

where random variables c, C_p, E_Z, and G are the analysis constant, pressure coefficient, exposure coefficient, and gust factor, respectively. V_{25} is the wind velocity of 25m/s, which is a deterministic variable. Statistical characteristics of random variables are given in Table 5.1. Values of COV of the pressure coefficient

and exposure coefficient for short- to medium-span bridges are different with those for long-span bridges. Statistical characteristics of the wind load effect caused by the wind velocity of 25m/s are decided through MCS and it is assumed that all random variables of Eq. (5.1) are statistically independent each other.

5.1.2 Distribution Type of Wind Load Effect Induced by Wind Velocity of 25m/s

A distribution type of the wind load effect caused by the wind velocity of 25m/s is verified by the K-S test with a significance level of 0.01. Candidates of the distribution type are normal, lognormal, Gumbel, and gamma distributions and parameters of each distribution are estimated by the method of moments. The K-S test of each candidate of the distribution type is conducted for short-to medium-span and long-span bridges, separately. The each K-S test is performed six times through MCS with the sample size from 10^1 to 10^6. The distribution type of the wind load effect induced by the wind velocity of 25m/s is determined with the maximum sample size where at least any distribution type is accepted among

Table 5.1 Statistical characteristics of random variables in the formula for the wind load effect (Ellingwood *et al*., 1980; Hong et al., 2009; Kim, 2018)

Random variable		Bias factor	COV		Distribution type
			Short- to medium-span	Long-span	
Analysis constant	c	1.00	0.050	0.050	Normal
Pressure coefficient	C_p	1.00	0.120	0.075	Normal
Exposure coefficient	E_Z	1.00	0.120	0.075	Normal
Gust factor	G	1.00	0.110	0.110	Normal

candidates of the distribution type.

The distribution types of the wind load effect caused by the wind velocity of 25m/s for short- to medium-span and long-span bridges are both decided as gamma distributions with the maximum sample size of 10^6.

5.1.3 Statistical Parameters of Wind Load Effect Induced by Wind Velocity of 25m/s

Statistical parameters of the wind load effect caused by the wind velocity of 25m/s are estimated by the method of least squares. They are calculated by the first-order necessary condition of the object function of Eq. (3.4). Sample size is set to 10^6. In case of the wind load effect induced by the wind velocity of 25m/s, statistical parameters θ_1 and θ_2 of Eq. (3.4) are the shape and scale parameters, respectively, since it follows a gamma distribution.

Values of mean and STD of the wind load effect caused by the wind velocity of 25m/s are computed using the statistical parameters by the method of moments and given in Table 5.2. Here, values of nominal of random variables of Eq. (5.1) are set to 1.00. The values of COV, nominal, and bias factor are also shown in the table. Therefore, bias factor and COV are decided to 1.00 and 0.21 for short- to medium-span bridges and 1.00 and 0.16 for long-span bridges.

Table 5.2 Values of mean, STD, COV, nominal, and bias factor of the wind load effect induced by the wind velocity of 25m/s

Type of bridge	Mean	STD	COV	Nominal	Bias factor
Short- to medium-span	624.7	130.9	0.210	625.0	1.000
Long-span	624.8	100.8	0.161	625.0	1.000

5.2 Conditions for Calibration of Ultimate Limit State V

5.2.1 Target Reliability Index, Resistances, and Load Effects for Ultimate Limit State V

The target reliability index for the calibration of the ULS-V is set to 3.72 whose corresponding probability of failure is 10^{-4} since it was applied to determined load factors of the ULS-V for general long-span bridges in the KHBDC-C. In addition, moment of RC, steel, and PC are adopted as resistances. Statistical characteristics used for reliability analyses are given in Tables 4.1 and 4.2 and those of the wind load effect induced by the wind velocity of 25m/s are presented in Section 5.1.

5.2.2 Ranges of DC-total Load Ratio and Wind Load Ratio

The ranges of the DC-total load ratio for the calibration are $-0.6 \le \theta \le 0.0$ and $0.0 \le \theta \le 0.6$ and Eq. (2.13b) are integrated with respect to the DC-total load ratio by the right Riemann sum in the range of $-0.6 \le \theta \le 0.0$ and the left Riemann

sum in the range of $0.0 \le \theta \le 0.6$ with the integration interval of 0.1. These ranges are determined based on the DC-total load ratio of moment at the bottom of pylons of the five existing cable-supported bridges in Korea, the YSB, the UB, the NMB, the IB, and the BHB. Load compositions of moment at the bottom of pylons generated by transverse wind loads applying the model 1 of the design lane load in the KHBDC-C and the proposed design lane load are given in Tables 5.3 and 5.4, respectively (Kim *et al*., 2017). The range of $-0.6 \le \theta \le 0.0$ is the case for which directions of effects induced by the *DC* and the other loads are opposite while the range of $0.0 \le \theta \le 0.6$ is the case for which directions of effects induced by the *DW* and the other loads are opposite. On the other hand, the assumption that a sum of load effects induced by the *DC* and *DW* is zero is verified by load compositions in Tables 5.3 and 5.4.

Table 5.3 Load composition of moment on the bottom of pylons of cable-supported bridges in Korea generated by transverse wind loads applying the model 1 of the design lane load in the KHBDC-C

Bridge		Moment (MN·m)					Variable	
		DC	*DW*	*LL*	WS_{25}	Total	Wind load ratio (χ)	DC-total load ratio (θ)
YSB		209.5	-209.0	505.2	489.2	994.9	0.4917	0.2106
UB		78.1	-81.5	250.2	144.5	391.3	0.3693	0.1996
NMB	Side	42.9	-42.9	121.3	60.4	181.7	0.3324	0.2361
	Center	0.3	-0.3	825.5	214.4	1039.9	0.2062	0.0003
IB		87.2	-81.9	81.6	254.5	341.4	0.7455	0.2554
BHB		-63.4	79.7	99.3	306.5	422.1	0.7261	-0.1502

Table 5.4 Load composition of moment on the bottom of pylons of cable-supported bridges in Korea generated by transverse wind loads applying the proposed design lane load

Bridge		Moment (MN·m)					Variable	
		DC	*DW*	*LL*	WS_{25}	Total	Wind load ratio (χ)	DC-total load ratio (θ)
YSB		209.5	-209.0	387.1	489.2	876.8	0.5579	0.2389
UB		78.1	-81.5	223.1	144.5	364.2	0.3968	0.2144
NMB	Side	42.9	-42.9	92.5	60.4	152.9	0.3950	0.2806
	Center	0.3	-0.3	628.4	214.4	842.8	0.2544	0.0004
IB		87.2	-81.9	67.6	254.5	327.4	0.7773	0.2663
BHB		-63.4	79.7	83.9	306.5	406.7	0.7536	-0.1559

The range of the wind load ratio in Eq. (2.13b) is $0.2 \le \chi \le 0.8$ and the equation is integrated with respect to the wind load ratio by the 5-point Gauss quadrature with the integration interval of 0.025. The range of $0.2 \le \chi \le 0.8$ is decided based on the wind load ratio of moment at the bottom of pylons of the five existing cable-supported bridges in Korea, shown in Tables 5.3 and 5.4.

5.3 Determination of L-R factors for Ultimate Limit State V

5.3.1 Calibration Process of Ultimate Limit State V

Four calibrations of the ULS-V are conducted by adopting the current or new statistical model of the vehicular live load effect and applying the statistical models of the wind load effect induced by the wind velocity of 25m/s for short- to

medium-span or long-span bridges. In the calibration of the ULS-V, the load factors of *LL* and WS_{25} are calculated for the range of $0.2 \le \chi \le 0.8$ by fixing the proposed resistance factors for moment and suggested load factors of *DC* and *DW* by the calibration for the ULS-I.

In case of short- to medium-span bridges, the maximum load factor of *DW* and minimum load factor of *DC* are fixed in the range of $-0.6 \le \theta \le 0.0$ while the maximum load factor of *DC* and minimum load factor of *DW* are hold in the range of $0.0 \le \theta \le 0.6$. Here, *DC* for cast-in-place members is applied since it is mostly used for designing short- to medium-span bridges. For long-span bridges, the load factor of *DW* suggested in the range of $0.0 \le \xi \le 0.6$ and minimum load factor of *DC* are fixed in the range of $-0.6 \le \theta \le 0.0$ while the load factor of *DC* proposed in the range of $0.0 \le \xi \le 0.6$ and minimum load factor of *DW* are hold in the range of $0.0 \le \theta \le 0.6$. In case of long-span bridges, *DC* for factory-made members is applied because it is mainly used to design.

A set of load factors of *LL* and WS_{25} is optimized in each range of the DC-total load ratio and a set of load factors is suggested for the ULS-V in common for both ranges of the DC-total load ratio. The proposed load factors are decided where the average of the reliability index over DC-total load ratios, member types, and wind load ratios applying the suggested load factors satisfies the target reliability index the most closely in both ranges of the DC-total load ratio.

5.3.2 Proposed Load Factors for Ultimate Limit State V

The optimized and proposed values of the load factors are given in Tables 5.5 and 5.6 for short- to medium-span and long-span bridges, respectively, with the load factors in the KHBDCs (MOLIT, 2016a; MOLIT, 2016b). In Table 5.5, the wind factor in the KHBDC is the equivalent load factor for the wind load effect induced by the wind velocity of 25m/s since the wind load effect of the ULS-V in the KHBDC is caused by the wind velocity which is the same with that in the ULS-I not 25m/s. Load factors of *LL* proposed by the new statistical model of the vehicular live load effect are less than those suggested by the current statistical model.

Table 5.5 The current, optimized, and proposed load factors of the ULS-V for short- to medium-span bridges

DC-total load ratio	Load factor		KHBDC	Current Q_{LL}		New Q_{LL}	
				Opt.	Prop.	Opt.	Prop.
$-0.6 \le \theta \le 0.0$	γ_{DC}	CIP	0.90	0.850	0.85	0.900	0.90
	γ_{DW}		1.50	1.600	1.60	1.550	1.55
	γ_{LL}		1.40	1.425	1.50	1.294	1.35
	$\gamma_{WS_{25}}$		1.40*	1.393	1.45	1.482	1.55
$0.0 \le \theta \le 0.6$	γ_{DC}	CIP	1.25	1.300	1.30	1.350	1.35
	γ_{DW}		0.65	0.750	0.75	0.800	0.80
	γ_{LL}		1.40	1.490	1.50	1.337	1.35
	$\gamma_{WS_{25}}$		1.40*	1.460	1.45	1.527	1.55

* Equivalent load factors for the wind load effect induced by the wind velocity of 25m/s

Table 5.6 The current, optimized, and proposed load factors of the ULS-V for long-span bridges

DC-total load ratio	Load factor	KHBDC-C	Current Q_{LL}		New Q_{LL}	
			Opt.	Prop.	Opt.	Prop.
$-0.6 \le \theta \le 0.0$	γ_{DC} FM	0.85	0.850	0.85	0.900	0.90
	γ_{DW}	1.25	1.150	1.15	1.200	1.20
	γ_{LL}	1.40	1.591	1.60	1.425	1.45
	$\gamma_{WS_{25}}$	1.70	1.319	1.35	1.381	1.40
$0.0 \le \theta \le 0.6$	γ_{DC} FM	1.15	1.050	1.05	1.100	1.10
	γ_{DW}	0.80	0.750	0.75	0.800	0.80
	γ_{LL}	1.40	1.605	1.60	1.439	1.45
	$\gamma_{WS_{25}}$	1.70	1.333	1.35	1.395	1.40

5.3.3 Results of Reliability Analyses by Proposed L-R Factors of Ultimate Limit State V

Figures 5.1 and 5.2 show the variation of the reliability index for moment with the wind load ratio of $0.2 \le \chi \le 0.8$ in the ranges of $-0.6 \le \theta \le 0.0$ and $0.0 \le \theta \le 0.6$, respectively, for six DC-total load ratios adopting the proposed L-R factors for short- to medium-span bridges by the current model of the vehicular live load effect. Here, six DC-total load ratios are the right-end points for the integration of Eq. (2.13b), -0.5000, -0.4000, -0.3000, -0.2000, -0.1000, and -0.0001, by the right Riemann sum in the range of $-0.6 \le \theta \le 0.0$ while those are the left-end points for the integration of Eq. (2.13b), 0.0001, 0.1000, 0.2000, 0.3000, 0.4000, and 0.5000, by the left Riemann sum in the range of $0.0 \le \theta \le 0.6$. Figures

from 5.3 to 5.6 illustrate the average reliability index over six DC-total load ratios for three member types. The average reliability index satisfies the target reliability index within ± 14% error bounds.

In addition, the average of the reliability index over six DC-total load ratios and three member types is plotted in Figures 5.7 and 5.8 for short- to medium-span and long-span bridges, respectively. The average reliability index by proposed L-R factors assures the target reliability more than that by L-R factors in the KHBDCs.

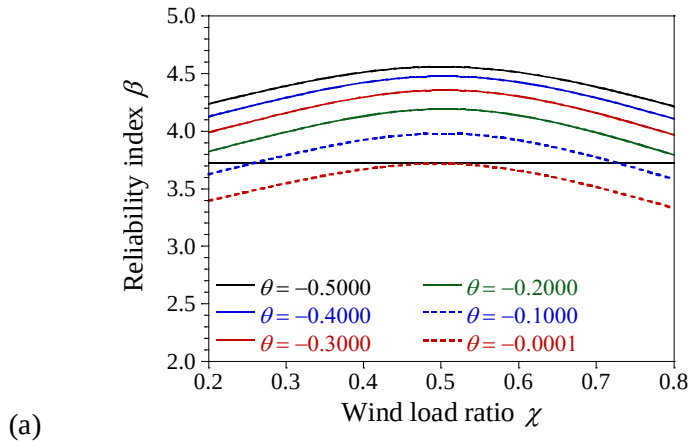

(a)

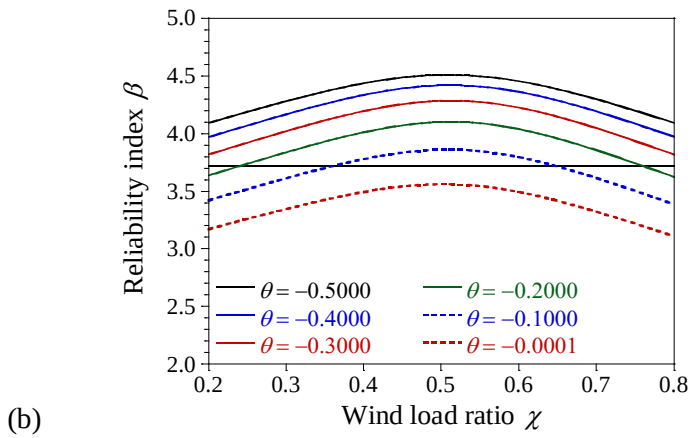

(b)

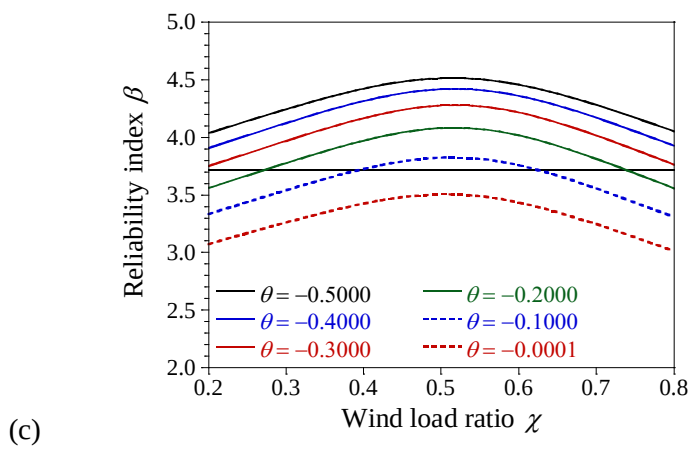

(c)

Figure 5.1 Variation of the reliability index for moment with the wind load ratio of $0.2 \le \chi \le 0.8$ in the range of $-0.6 \le \theta \le 0.0$ applying the proposed L-R factors for short- to medium-span bridges by the current model: (a) RC, (b) Steel, (c) PC

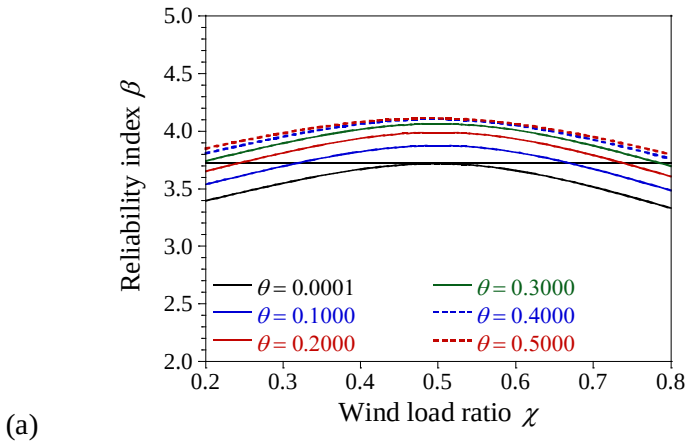

(a)

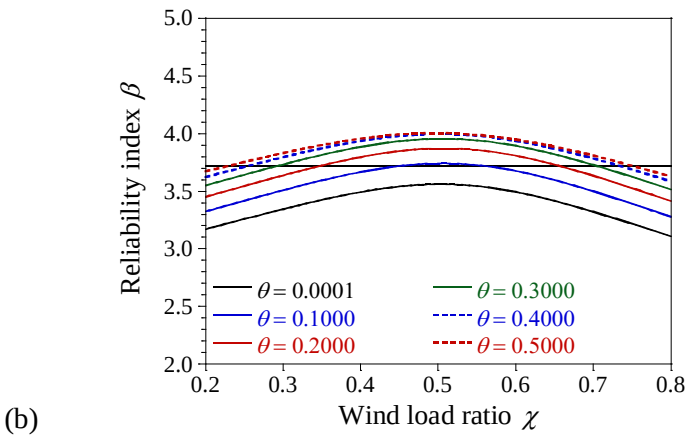

(b)

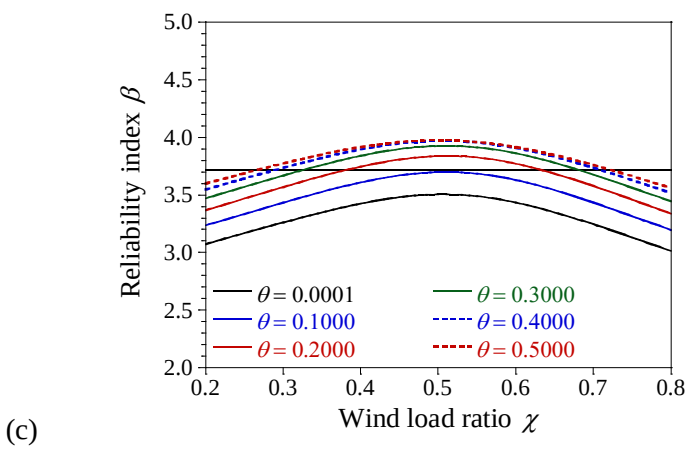

(c)

Figure 5.2 Variation of the reliability index for moment with the wind load ratio of $0.2 \le \chi \le 0.8$ in the range of $0.0 \le \theta \le 0.6$ applying the proposed L-R factors for short- to medium-span bridges by the current model: (a) RC, (b) Steel, (c) PC

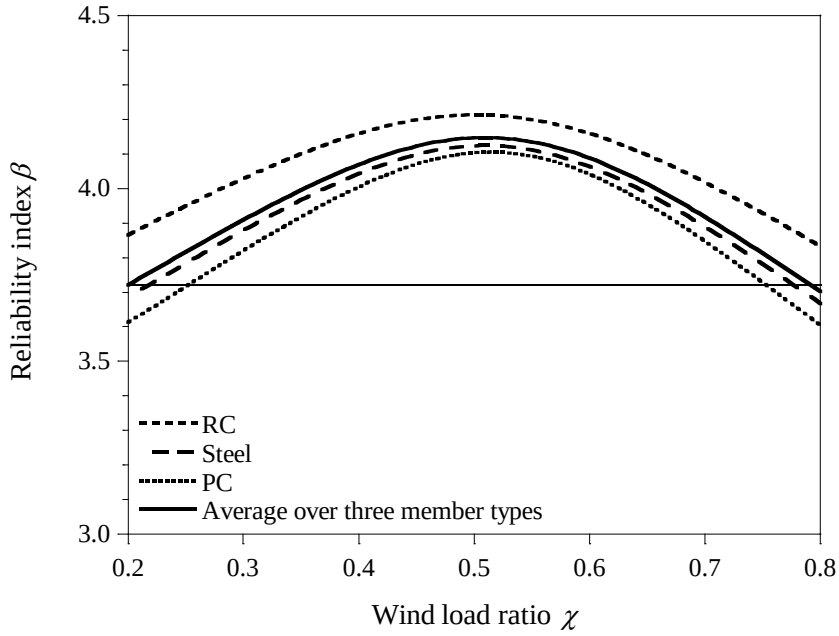

(a)

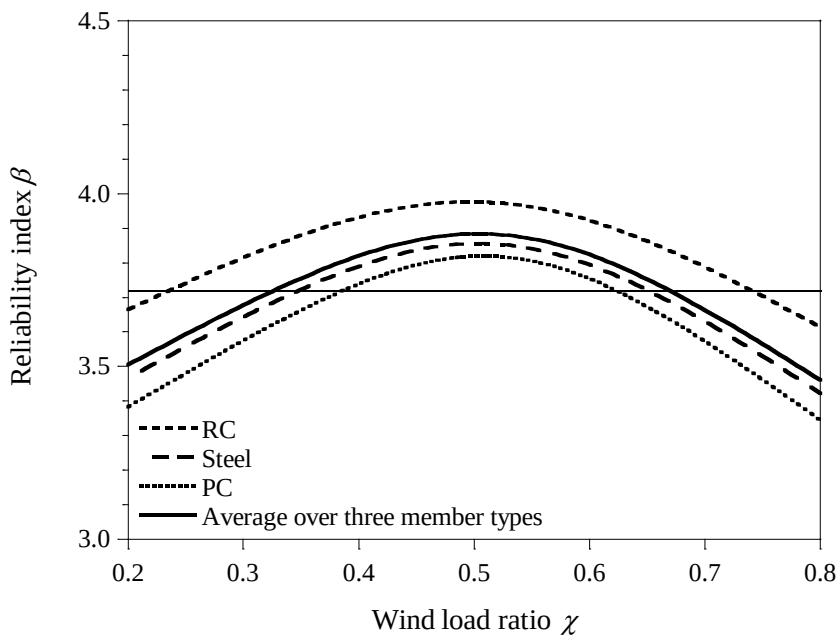

(b)

Figure 5.3 Variation of the average reliability index for moment over six DC-total load ratios with the wind load ratio of $0.2 \le \chi \le 0.8$ applying the proposed L-R factors for short- to medium-span bridges by the current model: (a) In the range of $-0.6 \le \theta \le 0.0$, (b) In the range of $0.0 \le \theta \le 0.6$

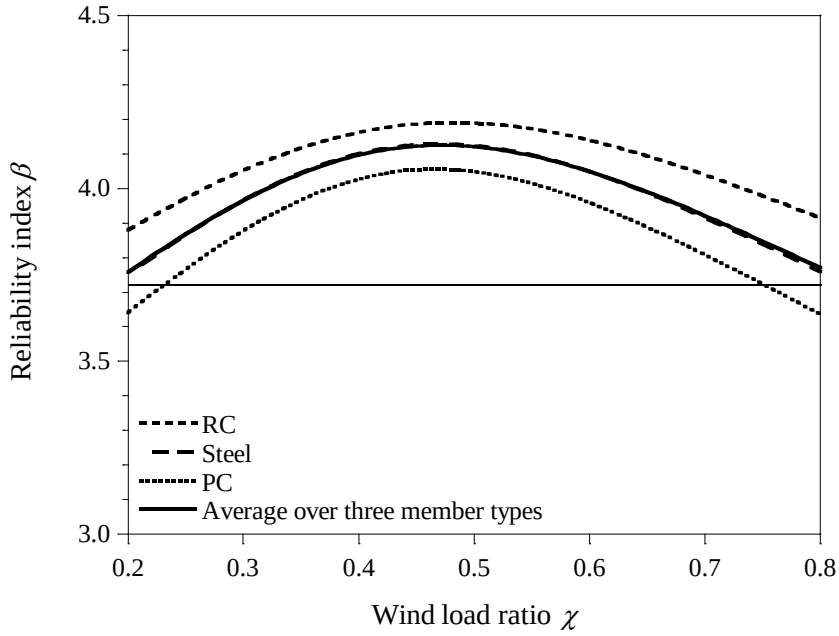

(a)

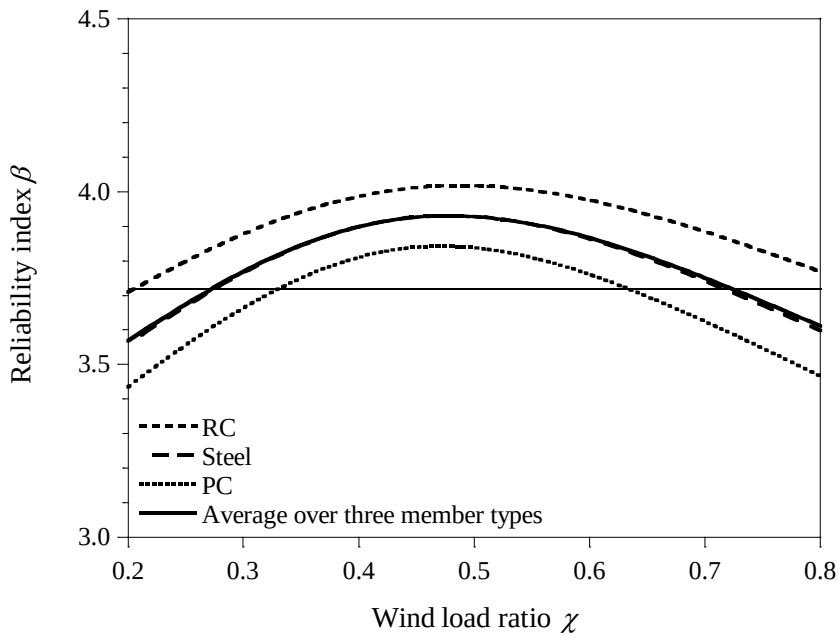

(b)

Figure 5.4 Variation of the average reliability index for moment over six DC-total load ratios with the wind load ratio of $0.2 \le \chi \le 0.8$ applying the proposed L-R factors for short- to medium-span bridges by the new model: (a) In the range of $-0.6 \le \theta \le 0.0$, (b) In the range of $0.0 \le \theta \le 0.6$

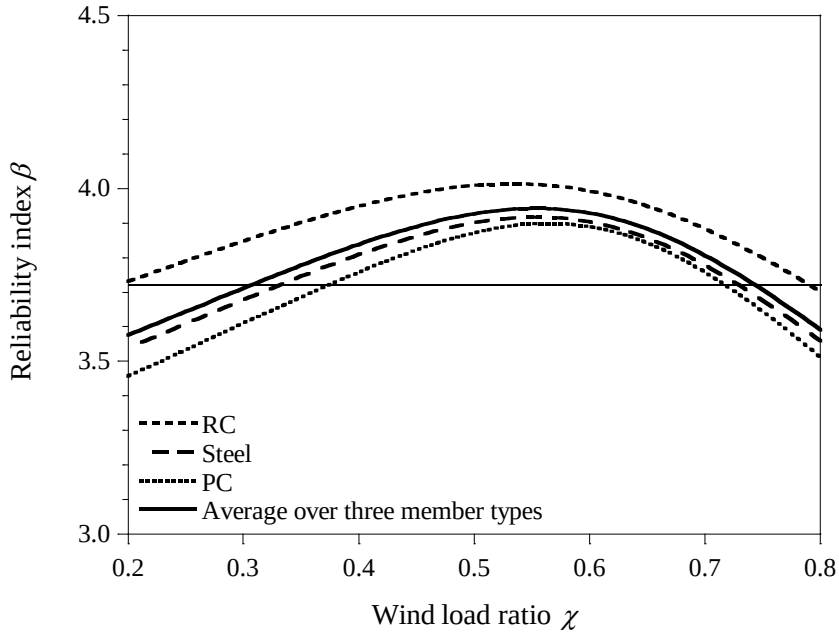

(a)

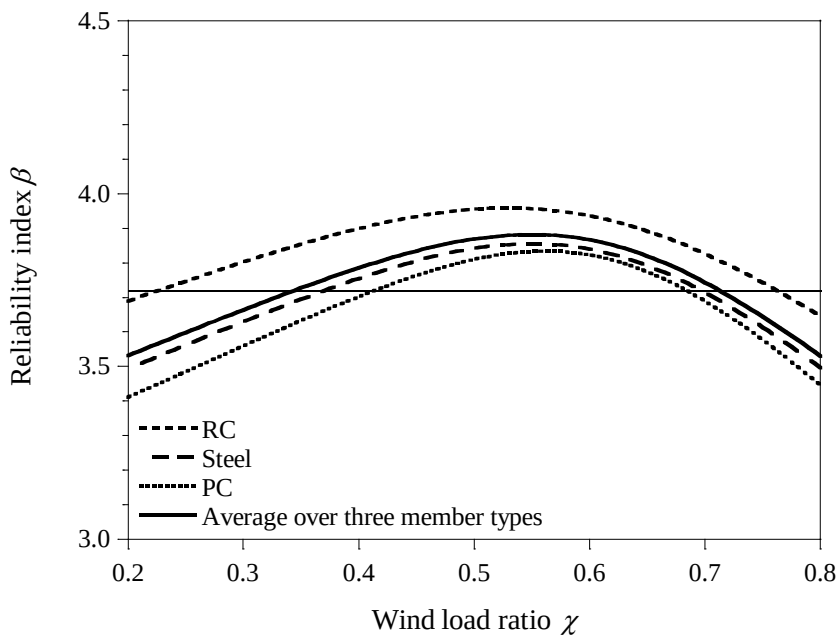

(b)

Figure 5.5 Variation of the average reliability index for moment over six DC-total load ratios with the wind load ratio of $0.2 \le \chi \le 0.8$ applying the proposed L-R factors for long-span bridges by the current model: (a) In the range of $-0.6 \le \theta \le 0.0$, (b) In the range of $0.0 \le \theta \le 0.6$

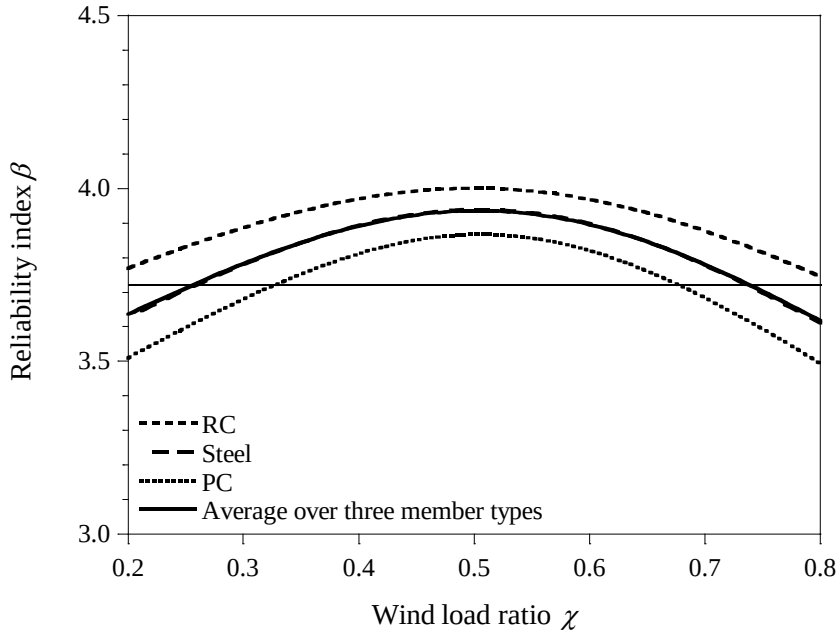

(a)

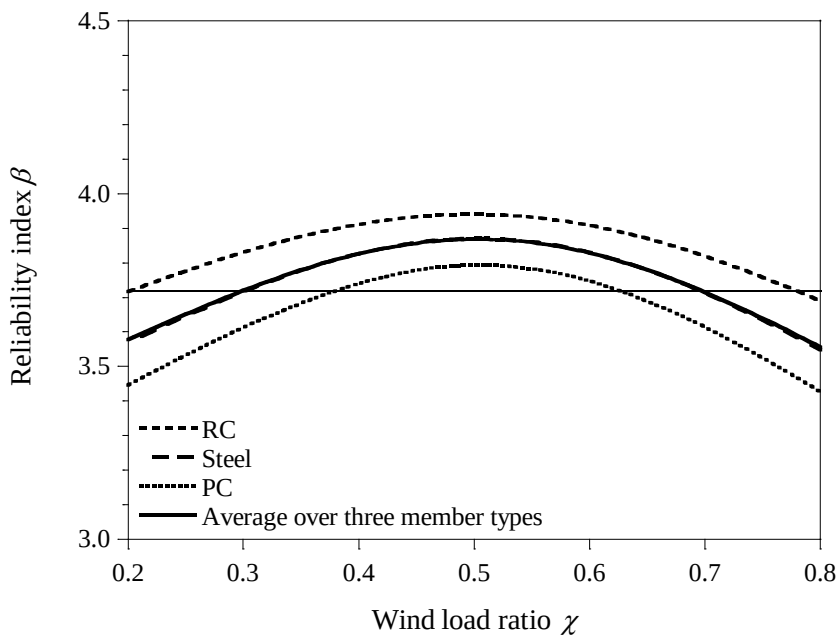

(b)

Figure 5.6 Variation of the average reliability index for moment over six DC-total load ratios with the wind load ratio of $0.2 \le \chi \le 0.8$ applying the proposed L-R factors for long-span bridges by the new model: (a) In the range of $-0.6 \le \theta \le 0.0$, (b) In the range of $0.0 \le \theta \le 0.6$

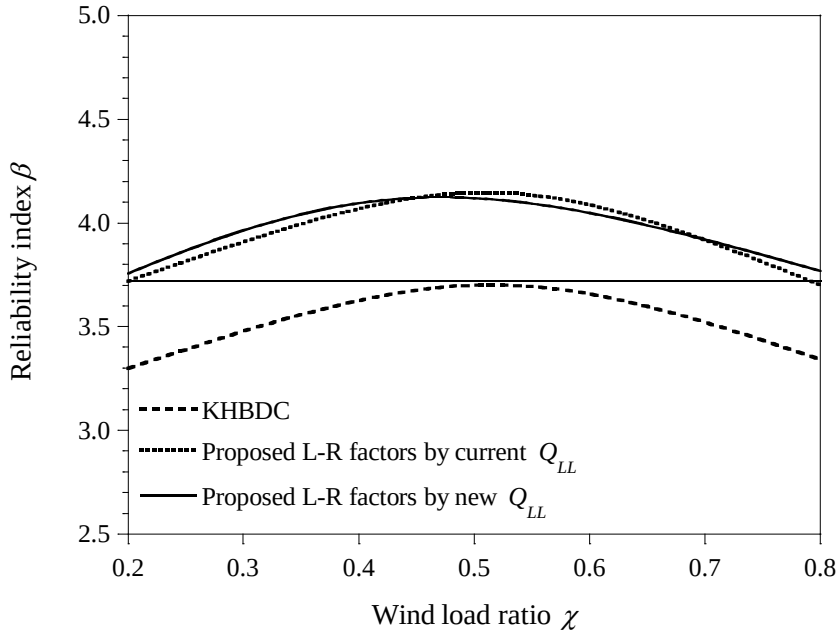

(a)

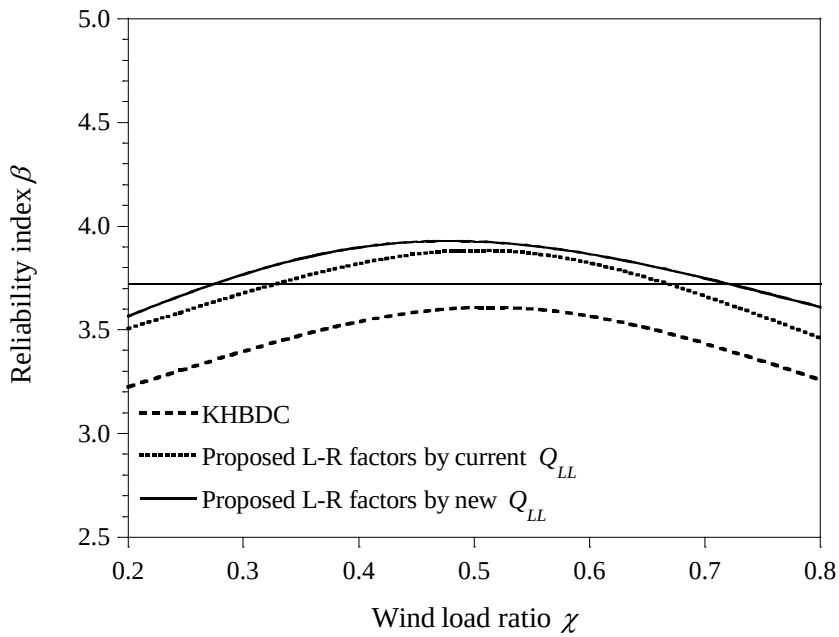

(b)

Figure 5.7 Variation of the average reliability index for moment over six DC-total load and three member types with the wind load ratio of $0.2 \le \chi \le 0.8$ applying the current and proposed L-R factors for short- to medium-span bridges: (a) In the range of $-0.6 \le \theta \le 0.0$, (b) In the range of $0.0 \le \theta \le 0.6$

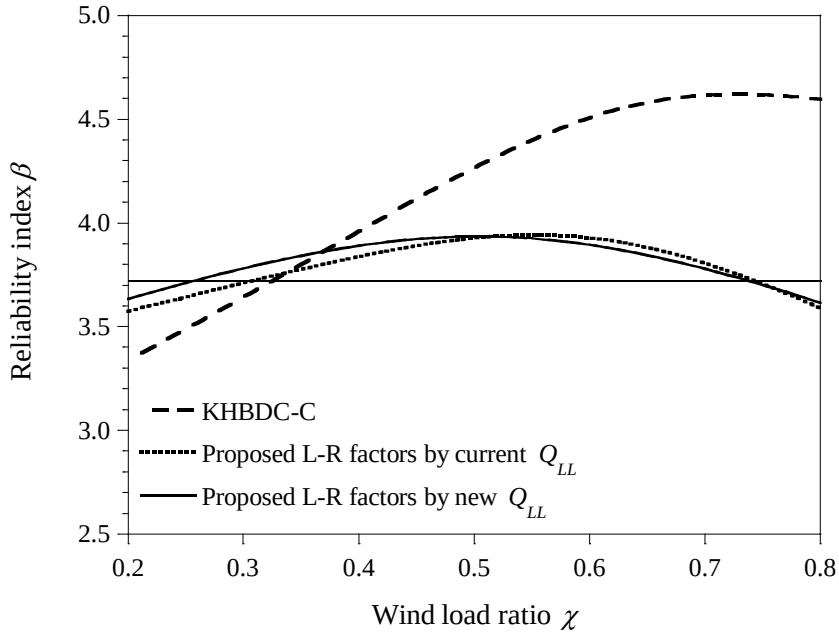

(a)

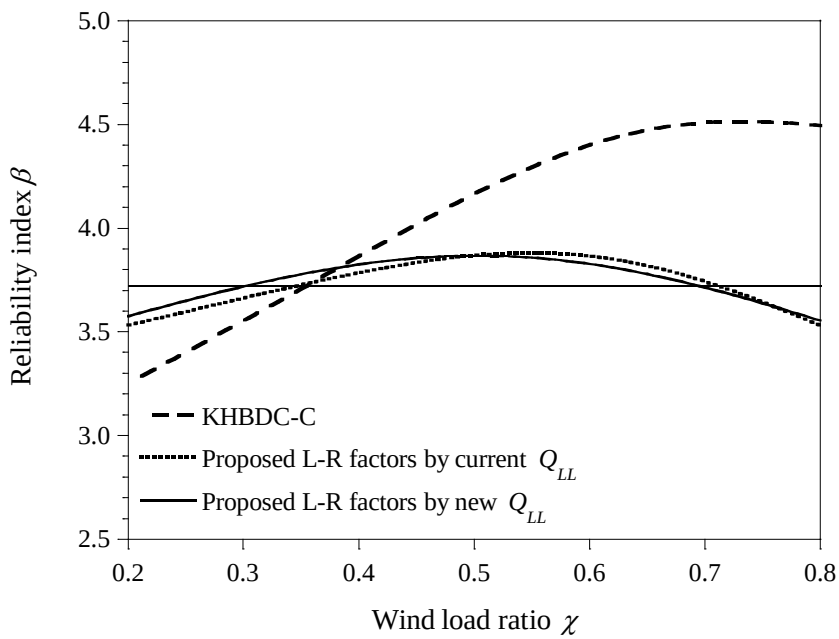

(b)

Figure 5.8 Variation of the average reliability index for moment over six DC-total load and three member types with the wind load ratio of $0.2 \le \chi \le 0.8$ applying the current and proposed L-R factors for long-span bridges: (a) In the range of $-0.6 \le \theta \le 0.0$, (b) In the range of $0.0 \le \theta \le 0.6$

6. CONCLUSIONS

The unified code calibration is conducted for the ULS-I and V applying the current and new statistical models of the vehicular live load effect. It is performed by adopting the optimization scheme developed by Lee *et al*. (2017) for uniformly satisfying the target reliability index.

The new statistical models of the vehicular live load and its effect are proposed base on WIM data in Korea for the calibration. Statistical characteristics are decided by performing MCS and the K-S test. The corresponding design lane load and multiple presence factors are suggested using the same data with the new statistical model of the vehicular live load effect so there is consistency of the design lane load and the live load factors which are decided by applying the new statistical model of the vehicular live load effect.

Load factors for the ULS-I and resistance factors are suggested and the load factors are depends on a range of dead load ratio. Ranges of the dead load ratio are decided considering the dead load ratio of existing cable-supported bridges in Korea. Load factors of *LL* proposed by the new statistical model of the vehicular live load effect are mostly less than those suggested by the current one while the load factors of *DC* and *DW* are in reverse because the new statistical model is less skewed and variable than the current one. Reliability indices evaluated by proposed L-R factors more uniformly satisfy the target level of reliability than those

calculated by L-R factors in the KHBDCs. Nevertheless, the load factors of the KHBDC-C is applicable in the range of $0.0 \le \xi \le 0.8$ since the average reliability index evaluated by L-R factors is within acceptable error bounds of the target reliability index in the range.

In the calibration of the ULS-V, load factors are suggested with proposing statistical models of the wind load effect induced by the wind velocity of 25m/s. Calibrations applying the current and new statistical models of the vehicular live load effect are conducted, respectively. Ranges of the wind load ratio and DC-total load ratio are determined based on load compositions of existing cable-supported bridges in Korea. Reliability indices evaluated by proposed L-R factors uniformly assure the target reliability index.

The results of the calibration may be applied in newer versions of the KHBDCs. However, it should be preceded to collect accurate statistical characteristics of load effects and resistances for conducting a robust calibration. Moreover, it is necessary to decide reasonable ranges of load compositions for an optimization. Then, the proposed L-R factors could be adopted to revise the KHBDCs with agreements of bridge designers.

REFERENCES

American Association of State Highway and Transportation Officials (AASHTO). (2014). *AASHTO LRFD Bridge Design Specifications*, AASHTO, Washington, DC.

Ang, A. H-S. and Tang, W. H. (2007). *Probability Concepts in Engineering: Emphasis on Applications to Civil and Environmental Engineering*, John Wiley & Sons, Inc., Hoboken, NJ.

Bae, C. (2016). *Determination of the Load-Resistance Factors for Reliability-Based Codes by Optimization*, M.S. Thesis, Seoul National University, Seoul, South Korea.

Ellingwood, B. R., Galambos, T. V., MacGregor, J. G., and Cornell, C. A. (1980). *Development of a Probability Based Load Criterion for American National Standard A58*, Washington, DC.

Haldar, A. and Mahadevan, S. (2000). *Probability, Reliability and Statistical Methods in Engineering Design*, John Wiley & Sons, Inc., New York.

Hong, H. P., Hu, Z., and King, J. P. C. (2009). Gust response of bridges to spatially varying wind excitations and calibration of wind load factors. *HIIFP-075*, Highway Standards Branch, Ontario Ministry of Transportation.

Hwang, E. S. (2012). *Development of Live Load Model for Long Span Bridges. Economic Design Technology for Long Span Cable Bridge*, Super Long Span Bridge R&D Center, Core Assignment 1, Detail Assignment 1, Research Report, Seoul National University (in Korean).

Kim, C. H. (2015). *Identification of Statistical Model of Vehicular Live Load in Long Span Bridges using WIM data*, M.S. Thesis, Seoul National University, Seoul, South Korea.

Kim, J. and Song, J. (2017). Full probabilistic model for traffic loads on bridges based on Weigh-In-Motion. *Proceedings of the 8th International Conference on Structural Health Monitoring of Intelligent Infrastructure*, Brisbane, Australia, 2017.

Kim, J. H. (2018). *Wind Load Factor Based on Wind Load Statistics for Reliability-Based Bridge Design Codes*, PhD Thesis, Seoul National University, Seoul, South Korea.

Kim, S., Kim, J. H., Song, S. W, and Lee, H. S. (2017). Determination of load-resistance factors for KHBDC based on new probabilistic models of live and wind loads. *Proceedings of 2017 KSCE Conference*, Busan, South Korea, 2017.

Lee, H. S., Bae, C., and Kim, J. H. (2017). Assessment of reliability levels and adjustment of load-resistance factors using optimization for gravitational loads-governed limit states of the AASHTO LRFD Bridge Design Specifications. *KSCE Journal of Civil Engineering*, DOI: 10.1007/s12205-017-0500-6

Lee, S. H. (2014). *Calibration of the Load-Resistance Factors for the Reliability-based Design of Cable-supported Bridges*, PhD Thesis, Seoul National University, Seoul, South Korea (in Korean).

Ministry of Land, Infrastructure and Transport (MOLIT). (2016a). *Korean Highway Bridge Design Code (Limit State Design)*, MOLIT, Seoul, South Korea (in Korean).

Ministry of Land, Infrastructure and Transport (MOLIT). (2016b). *Korean Highway Bridge Design Code (Limit State Design)- Cable-supported Bridges*, MOLIT, Seoul, South Korea (in Korean).

Nowak, A. S. (1999). *Calibration of LRFD bridge design code*, NCHRP Report 368, Transportation Research Board, Washington, D.C.

Nowak, A. S., Lutomirska, M., and Sheikh Ibrahim, F. I. (2010). The development of live load for long span bridges. *Bridge Structures*, Vol. 6, No. 1, 2, pp. 73-79.

Paik, I., Hwang, E. S., and Shin, S. (2009). Reliability analysis of concrete bridges designed with material and member resistance factors. *Computers and Concrete*, Vol. 6, No. 1, pp. 59-78.

Rackwitz, R. and Fiessler, B. (1978). Structural reliability under combined random load sequences. *Computers & Structures*, Vol. 9, No. 5, pp. 489-494.

Shin, D. K., Kim, C. Y., and Paik, I. (2006). Reliability analysis of composite girder designed by LRFD method for positive flexure. *Journal of the Korean Society of Civil Engineers*, Vol. 26, No. 3A, pp. 539-546 (in Korean).

This page intentionally left blank

초록

한국에는 일반교량과 장경간교량 각각에 대해 신뢰도 기반의 하중-저항계수 설계법을 바탕으로 한 교량설계기준이 있다. 일반교량을 위한 교량설계기준의 하중-저항계수와 장경간교량을 위한 교량설계기준의 하중-저항계수는 개별적으로 개발되었기 때문에 이에 대한 통합 코드캘리브레이션이 필요하다. 더욱이 설계 차량활하중의 이론적 배경과 차량활하중효과 확률모형의 이론적 배경의 일관성이 부족한 실정이다. 따라서 동일한 데이터를 기반으로 새로운 차량활하중효과 확률모형과 그에 상응하는 설계 차로하중을 제안하고, 극한한계상태 I과 극한한계상태 V에 대한 통합 코드캘리브레이션을 수행한다. 이때, 기존의 차량활하중효과 확률모형을 적용한 통합 코드캘리브레이션과 새로운 차량활하중효과 확률모형을 적용한 통합 코드캘리브레이션을 각각 수행한다. 코드캘리브레이션은 목표신뢰도 수준을 균일하게 만족하게 하기 위해 최적화 기법을 적용하여 수행된다. 극한한계상태 I의 하중계수는 하중구성에 따라 정의되므로 제안 하중-저항계수는 일반교량의 설계뿐만 아니라 장경간교량의 설계에도 적용 가능하다. 그리고 극한한계상태 V의 캘리브레이션은 일반교량과 장경간교량에 대해 각각 수행된다. 제안 하중-저항계수에 의해 계산된 신뢰도지수는

현재 설계기준의 하중-저항계수에 의해 계산된 신뢰도지수에 비해 목표신뢰도지수를 더 균일하게 만족한다.

주요어 : 코드 캘리브레이션, 하중-저항계수, 극한한계상태 I,
극한한계상태 V, 도로교설계기준(한계상태설계법),
차량활하중효과 확률모형, 일반교량, 장경간교량, 최적화 기법

학 번 : 2016-21245